Multichannel Analysis of Surface Waves
Methods for dispersion analysis of surface wave data

Elín Ásta Ólafsdóttir

December 2014

Contents

List of Figures

List of Tables

Chapter 1

Introduction

1.1 Background

Knowledge of the geotechnical properties of subsoil sites, such as the stiffness of the top-most soil layers, is essential in various civil and earthquake engineering projects. Several different methods can be applied to estimate the stiffness of soils. Among those are drilling methods such as *down-hole* and *cross-hole seismic surveys*, methods where the resistance of soil to penetration is measured like the *standard penetration test (SPT)* and the *cone penetration test (CPT)* and *surface wave analysis methods*. In surface wave methods, Rayleigh-type surface waves are generated and used to infer the shear wave velocity profile of the test site as a function of depth. The shear wave velocity of individual soil layers is directly proportional to their shear modulus, which is their stiffness. Compared to other available methods, surface wave methods are low-cost, as well as being non-invasive and environmental-friendly since they neither require heavy machinery and nor leave lasting marks on the surface of the test site. Moreover, surface wave methods have been shown to provide consistently reliable results (Park, Miller & Xia, 1997; Xia et al., 2002). Surface wave analysis methods for estimating shear wave velocity/stiffness of subsoil sites are therefore of great interest.

The dispersive nature of Rayleigh-type surface waves in layered medium provides key information regarding the properties of near-surface materials. The basis of most surface wave analysis methods is an accurate determination of the frequency-dependent phase velocity of the fundamental mode of Rayleigh waves (Park et al., 1997). Apart from being a function of frequency, the Rayleigh wave phase velocity is related to several groups of Earth's properties, most importantly the shear wave velocity of individual soil layers. Thus, by inverting the dispersive phase velocity of recorded Rayleigh waves, the shear wave velocity profile for the test site can be obtained (Xia, Miller & Park, 1999). The shear wave velocity profile can then be used to evaluate the stiffness of the top-most soil layers. Furthermore, in earthquake design the shear wave velocity is a vital parameter in both liquefaction potential and soil amplification assessments and when defining site-specific earthquake design loading according to Eurocode 8 (Bessason & Erlingsson, 2011; Lin, Chang & Chang, 2004).

1

Several types of surface wave methods can be applied to extract Rayleigh wave dispersion curves from recorded surface wave data and utilize them to estimate the shear wave velocity profile of the top-most soil layers. Among them are *Spectral Analysis of Surface Waves (SASW)* and *Multichannel Analysis of Surface Waves (MASW)*. SASW measurements have been carried out in Iceland for almost two decades to estimate shear wave velocity profiles at both natural sites and in man-made fillings (Bessason & Erlingsson, 2011). However, the MASW method has until now never been used in Iceland.

The MASW method has several advantages over the SASW procedure. Data acquisition in the field is much less time consuming and the data processing is faster and easier to automate. Furthermore, noise sources, such as inclusion of body waves and reflected/scattered waves, can more easily be identified and eliminated as compared to the SASW method. Reduction of noise is of great importance, as it ultimately leads to a more precise shear wave velocity profile (Park, Miller & Xia, 1999; Xia et al., 2002). Moreover, observation of multi-modal dispersion characteristics and generation of two (or three) dimensional dispersion images becomes possible and economically feasible by using the MASW method (Park, Miller & Xia, 2001; Park, Miller, Xia & Ivanov, 2007; Xia, Miller, Park & Tian, 2003).

The MASW method can be divided into three main steps (Park et al., 1999):

1. *Data acquisition.*

2. *Dispersion analysis.* (Determination of a Rayleigh wave dispersion curve.)

3. *Inversion analysis.* (Determination of a shear wave velocity profile.)

The Engineering Research Institute, University of Iceland, (Verkfræðistofnun HÍ) purchased in 2013 a new set of 24 geophones along with a special connection cable and a data acquisition system for MASW field measurements based on grants from the Icelandic Road Administration (Rannsóknasjóður Vegagerðarinnar) and the Landsvirkjun Energy Research Fund (Orkurannsóknarsjóður). Data acquisition software was also developed. During the fall of 2013, the first MASW field measurements were carried out close to Arnarbæli in South Iceland. Development of a data processing program to perform the dispersion analysis, i.e. to extract Rayleigh wave dispersion curves from recorded multichannel surface wave data, began in fall 2013 and is now in its later stages. Work regarding the final step, inversion of Rayleigh wave dispersion curves, began in summer 2014.

The main objective of this report is to provide a comprehensive description of the two first steps of the MASW method. The second aim of this stage of the project is to develop a data processing program to extract Rayleigh wave dispersion curves from recorded multichannel surface wave data using the computational software Matlab. Later stages will include development of a data processing program to perform the inversion analysis involved in the MASW method.

1.2 Overview

The general outline of this report is as follows:

After introduction, Chapter 2 provides a general introduction to the main types of waves that propagate within the Earth and along its surface following a seismic disturbance. Emphasis is on Rayleigh waves and their dispersive properties. The relations between seismic wave velocities and the elastic moduli of the wave medium are also introduced.

Chapter 3 provides a short description of the SASW method. Emphasis is on data acquisition procedures and the general data processing methods used to obtain fundamental mode dispersion curves.

The main objective of Chapter 4 is to provide a general overview of the active MASW method. Passive MASW surveys are described shortly.

Chapter 5 describes the field procedures and the generally recommended data acquisition parameters for active MASW surveys. Emphasis is on surface wave generation and recording using an impulsive seismic source.

In Chapter 6, two methods to extract dispersion curves from recorded multichannel surface wave data are explained in detail; a swept-frequency approach by Park et al. (1999) and the phase-shift method by Park et al. (1998).

Chapter 7 provides a general overview of the inversion analysis involved in both MASW and SASW surveys.

Chapter 8 summarizes the main results of this report and the next steps of the project.

Appendix A contains supplementary information regarding the MASW test measurements that were carried out during the fall of 2013 close to Arnarbæli in South Iceland. Dispersion curves obtained from the recorded data, by using the phase-shift method and the swept-frequency approach, are presented and results obtained by the two methods are compared.

Chapter 2

Seismic waves

Following a seismic disturbance, several types of waves propagate within the Earth and along its surface. The waves generated can be divided into two main categories; *body waves* and *surface waves* (Evrett, 2013).

2.1 Body waves

Body waves are transmitted through the interior of the Earth, the medium of the wave, and consist of *compressional waves* (*P-waves/primary waves*) and *shear waves* (*S-waves/ secondary waves*). The particle motion associated with compressional waves is parallel to the motion of the wave itself, causing stretching and compressing of elementary volume particles, i.e. change in size, as shown in Figure 2.1 (Evrett, 2013).

The particle motion of shear waves is perpendicular to the direction of wave propagation and has therefore both a vertical and a horizontal component. The transverse particle motion causes shear deformation of volume elements within the medium, i.e. change in shape, as shown in Figure 2.2 (Aki & Richards, 2002; Evrett, 2013).
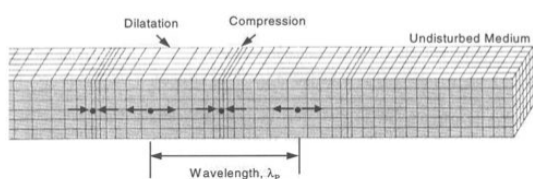
Figure 2.1: Particle motion associated with compressional waves (Bolt, 1976).
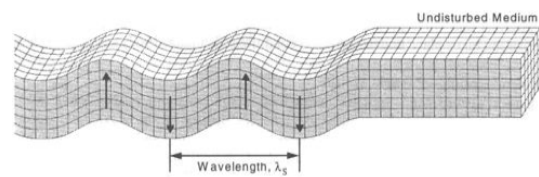
Figure 2.2: Particle motion associated with shear waves (Bolt, 1976).

2.2 Surface waves

Surface waves travel along the interface between two different media, i.e. near the surface of the Earth, and are the results of interfering P-waves and/or S-waves (Xia et al., 2002). There are two main types of surface waves; *Rayleigh waves* and *Love waves* (Evrett, 2013). The particle motion of Rayleigh waves is in a vertical direction and reminds of

rolling ocean waves (Evrett, 2013; Xia, Miller & Park, 1999), as shown in Figure 2.3. Rayleigh waves are discussed in more detail in Section 2.2.1.

The particle motion associated with Love waves is horizontal and transverse to the direction of wave propagation (Evrett, 2013), as shown in Figure 2.4. Love waves are only generated where there is a soft (low velocity) layer overlying a stiffer layer whereas Rayleigh waves always exist in the presence of a free surface (Foti, 2000).
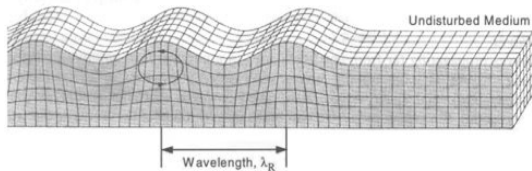
Figure 2.3: Particle motion associated with Rayleigh waves (Bolt, 1976).
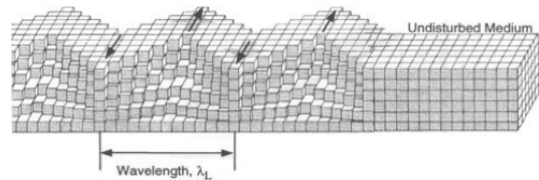
Figure 2.4: Particle motion associated with Love waves (Bolt, 1976).

2.2.1   Rayleigh waves

Rayleigh waves are the most fundamental of the surface waves (Aki & Richards, 2002) and are of great interest in near-surface geophysics as they can provide key information regarding the properties of the Earth's sub-surface (Evrett, 2013; Park et al., 1997; 1999). *Ground roll* is a particular type of Rayleigh waves that is characterized by relatively high amplitude and low frequency and travels along or very close to the surface of the Earth (Xia et al., 1999). Ground roll is the type of surface waves most effectively generated and recorded using vertical seismic sources and vertical receivers (Park et al., 1997).

A vertical seismic source, e.g. a sledgehammer impact or a vibrating plate, will radiate a combination of P-waves, S-waves and Rayleigh waves. Around two-thirds (67%) of the seismic energy will typically be imparted into Rayleigh waves (principally ground roll) while 23% is imparted into S-waves and 7% into P-waves (Evrett, 2013). Resulting from their horizontal particle motion, Love waves are seldom recorded in surveys in which only vertical sources and vertical receivers are used (Park et al., 1997).

Rayleigh waves cause surface particles of the medium to move along elliptical paths in the vertical plane consistent with the direction of wave propagation. The particle motion is retrograde elliptical near the surface, becoming prograde elliptical with increasing depth (Aki & Richards, 2002; Evrett, 2013), see Figure 2.5 (right).

The amplitude of Rayleigh waves decays exponentially with depth. At a penetration depth comparable to one wavelength, the displacement of the medium has become less than 30% of its surface value, see Figure 2.5 (left). If generated by a point source, the energy of the wave falls of as $1/r$, where r is the distance to the seismic source (Evrett, 2013). Thus, the in-plane amplitude of a Rayleigh wave decays as $1/\sqrt{r}$ if a point source is assumed (Young & Freedman, 2008).
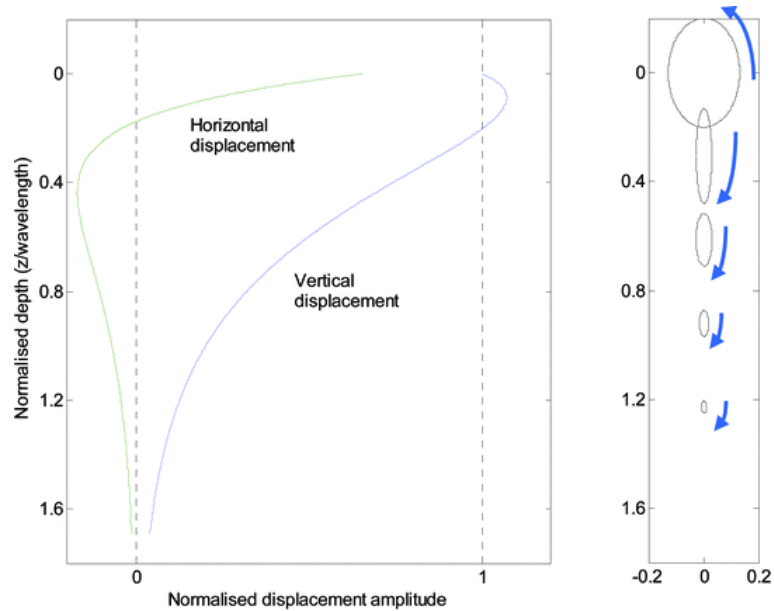
Figure 2.5: Displacement amplitude (left) and vertical particle motion (right) of Rayleigh waves as a function of depth (Gedge & Hill, 2012).

In a homogeneous half-space, the Rayleigh wave velocity is independent of frequency, i.e. Rayleigh waves do not disperse in a homogeneous medium. However, Rayleigh waves are dispersive in a layered medium; wave components with different wavelength (and therefore different frequency) have different penetration depths and propagate at different velocities. The propagation velocity of individual frequency components is referred to as *phase velocity* (V_R) (Evrett, 2013; Park et al., 1997). The *group velocity* (V_g) of the wave is the velocity at which the wave-packet envelope propagates through the medium (Evrett, 2013). This is shown in Figure 2.6. The blue dot moves with the phase velocity along the black path while the red wave-packet envelope propagates with the group velocity from left to right.
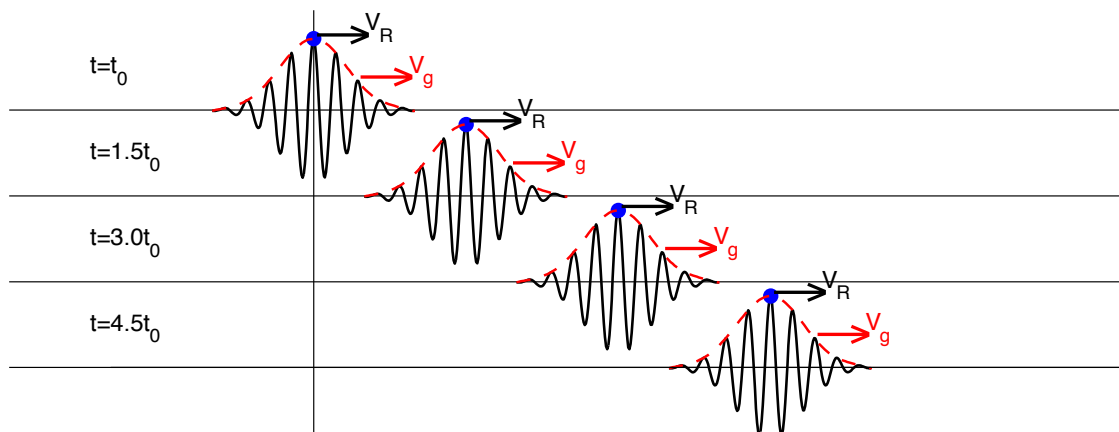
Figure 2.6: Comparison of Rayleigh wave phase velocity (V_R) and group velocity (V_g).

Dispersion of Rayleigh waves can be visualized by examining an idealized vibrating seismic source, vibrating at a single frequency f at the surface of a multilayered elastic medium. The wavelength λ of the resulting Rayleigh waves is constant and can be determined by measuring the distance between successive peaks (or troughs) in the observed surface wave motion. A low frequency source generates long-wavelength Rayleigh waves that excite multiple layers of the medium (see Figure 2.7 (a)), while seismic sources of a higher frequency generate Rayleigh waves with shorter wavelength and shallower penetration depth (see Figure 2.7 (b) and (c)) (Evrett, 2013).
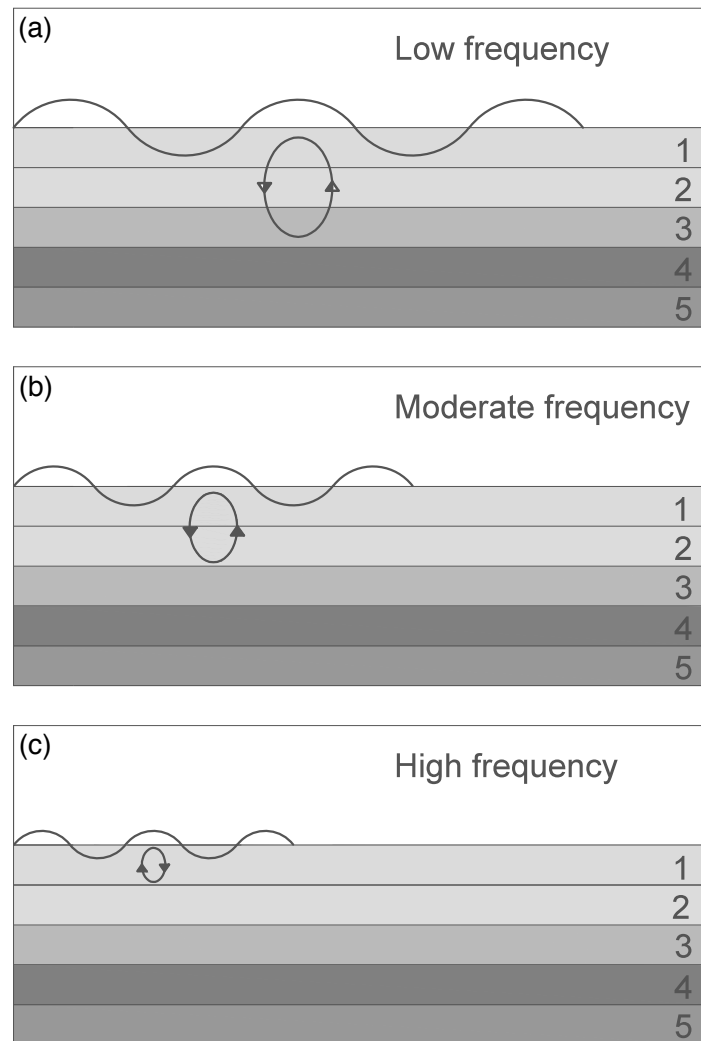
Figure 2.7: The penetration depth of Rayleigh waves depends on their wavelength and frequency. Low-frequency (long-wavelength) Rayleigh waves, (a), penetrate deeper than Rayleigh waves of higher frequencies (shorter wavelengths), (b) and (c).

The phase velocity of each wave component is primarily dependent on the elastic moduli of the layers that the wave component excites. Thus, in Figure 2.7 (c) only the elastic moduli of the top-most layer have impact on the Rayleigh wave phase velocity, whereas the phase velocity of the waves in Figure 2.7 (a) and (b) depends also on the elastic properties of deeper layers. Each mode of a given surface wave will therefore exhibit a unique phase velocity at each frequency (Evrett, 2013; Xia et al., 2002).

Generally, seismic velocities are observed to increase with depth, i.e. waves with longer wavelengths (lower frequency) propagate faster than waves with shorter wavelengths as indicated by Eq. (2.2.1) (Bessason & Erlingsson, 2001; Evrett 2013):

$$\lambda(f) = \frac{V_R(f)}{f} \tag{2.2.1}$$

where f is frequency, $V_R(f)$ is the phase velocity of Rayleigh wave components of frequency f and $\lambda(f)$ is the Rayleigh wave wavelength at frequency f.

A plot of frequency versus phase velocity, known as a *dispersion curve*, visualizes these relations (see Figure 2.8 (a)). The shape of the dispersion curve is referred to as the *dispersion characteristic* of the Rayleigh wave (Evrett, 2013).

Typically multiple phase velocities exist for a given frequency, making the dispersion curve multi-modal. The mode with the lowest phase velocity (at each frequency) is termed the *fundamental mode* (M_0). It exists at all frequencies. Higher modes, called *first mode* (M_1), *second mode* (M_2) etc., have higher phase velocities and are only present above a cut-off frequency that depends on the mode (Evrett, 2013) (see Figure 2.8 (b)).
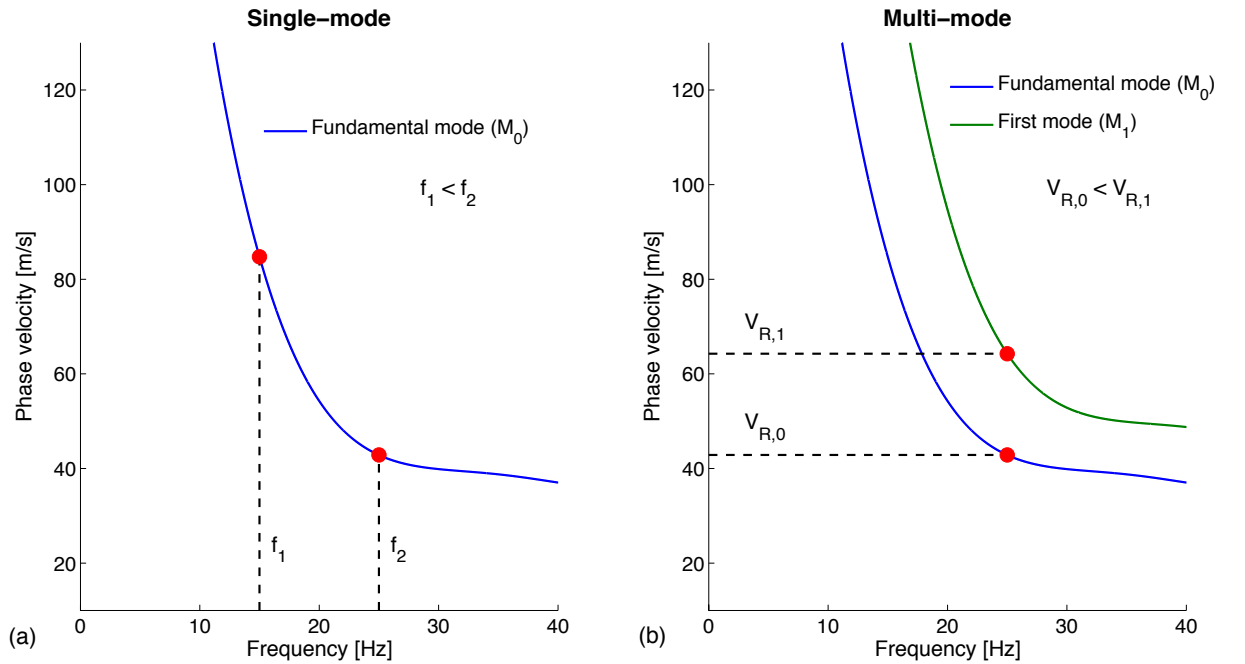
Figure 2.8: (a) Fundamental mode dispersion curve. (b) Fundamental mode and first mode dispersion curves.

2.3   Seismic wave velocity and elastic moduli

The body wave velocities of geomaterials; shear wave velocity (V_s) and compressional wave velocity (V_P), can be directly related to the elastic moduli of the medium which the waves propagate through. The relationships between the elastic moduli and the body wave velocities are widely utilized in geophysical surveys in order to gain information about the spatially distributed mechanical properties of subsoil sites (Evrett, 2013). The shear wave velocity (V_s) is especially a valuable indicator of the stress-strain behaviour of soil due to its relations to the small-strain shear modulus (G_{max}) (Wair, DeJong & Shantz, 2012).

The shear modulus of soil (G) is highly dependent upon strain level as indicated by the stress-strain curve shown in Figure 2.9. For small shear deformations the behaviour of soil is very close to being elastic, i.e. the shear modulus for small strains can be assumed to be constant at its maximum value, G_{max}. For increased deformation, the stiffness of soil diminishes as indicated by the decreasing slope of the stress-strain curve in Figure 2.9 (Kaldal, 2007; Luna & Jadi, 2000).
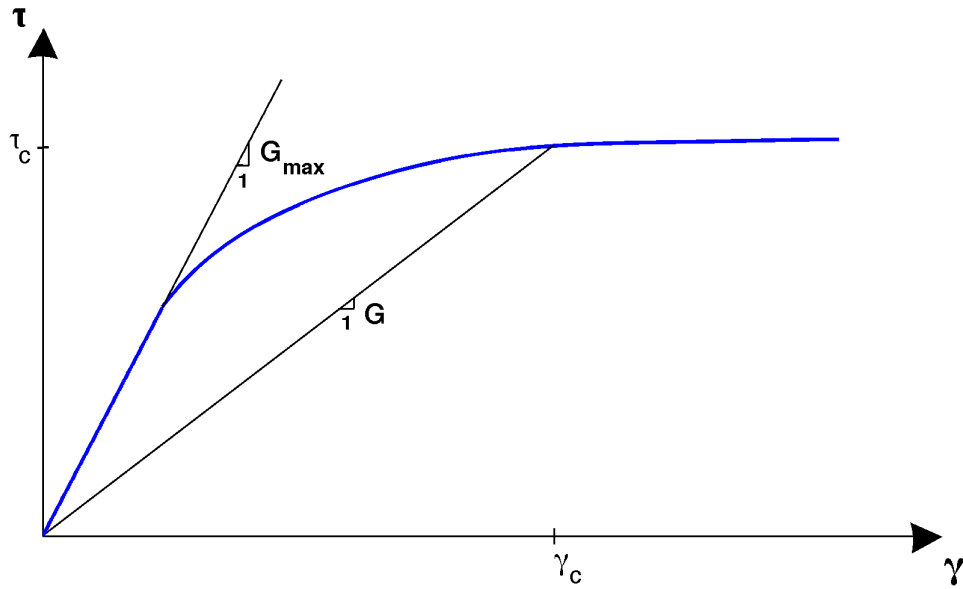
Figure 2.9: Stress-strain curve with variation of shear modulus (G). For small shear deformations G_{max} is obtained.

The shear strains induced by most geophysical seismic methods, such as SASW and MASW surveys, are small and well within the range where the behaviour of soil can be assumed elastic. The calculated shear wave velocity can therefore be used to infer the stiffness of the material through which the waves propagate, i.e.

$$G_{max} = \rho V_S^2 \qquad\qquad (2.3.1)$$

where ρ is the mass density of the soil (Kaldal, 2007; Luna & Jadi, 2000).

Based on the relations between the modulus of elasticity, (E) and the shear modulus (G) of homogeneous isotropic linearly elastic materials, the (small-strain) modulus of elasticity of the soil layers under study (E_{max}) can be estimated as (Evrett, 2013; Sigbjörnsson, 2007):

$$E_{max} = 2G_{max}(1 + \nu) = 2\rho V_S^2 (1 + \nu) \tag{2.3.2}$$

where ν is Poisson's ratio. For sandy or gravelly sites, the value of the Poisson's ratio is typically in the range of $\nu \approx 0.25 - 0.35$ (Bessason & Erlingsson, 2011).

By solving Eq. (2.3.2) for V_s the following equation is obtained:

$$V_S = \sqrt{\frac{G_{max}}{\rho}} = \sqrt{\frac{E_{max}}{2\rho(1 + \nu)}} \tag{2.3.3}$$

A similar expression exists for compressional wave velocity (V_P) (Evrett, 2013), i.e.

$$V_P = \sqrt{\frac{(1 - \nu)E_{max}}{(1 + \nu)(1 - 2\nu)\rho}} \tag{2.3.4}$$

By taking the ratio of Eqs. (2.3.3) and (2.3.4), the following relation between V_P and V_S is obtained (Evrett, 2013):

$$\frac{V_P}{V_S} = \sqrt{\frac{2(1 - \nu)}{1 - 2\nu}} \tag{2.3.5}$$

Thus, with a known shear wave velocity and a known (or guessed) Poisson's ratio, the compressional wave velocity can estimated by Eq. (2.3.5).

The Rayleigh wave velocity (V_R) is always lower than the shear wave velocity (V_S). The relation between V_R and V_S depends on the mechanical properties of the wave medium. The Rayleigh wave velocity for isotropic elastic solids was first approximated by Bergmann (as cited in Vink & Malischew, 2007) as:

$$V_R = \frac{0.87 + 1.12\nu}{1 + \nu} V_S \tag{2.3.6}$$

Thus, for a material with $\nu = 0.3$ the estimated Rayleigh wave velocity is:

$$V_R \approx 0.93 V_S \tag{2.3.7}$$

Chapter 3

Spectral Analysis of Surface Waves

The *Spectral Analysis of Surface Waves (SASW)* method was introduced in the early 1980s. The SASW method utilizes the dispersion characteristics of Rayleigh waves (i.e. ground roll) in a multi-layered medium to estimate the shear wave velocity of individual near-surface soil layers (Park et al. 1999, Xia et al. 1999). Surface waves are generated with an impulsive source and detected by geophones. The collected data is analyzed in the frequency domain to determine a dispersion curve. The dispersion curve is then used as a basis for the computation of a shear wave velocity profile as a function of depth for the given site (Bessason & Erlingsson, 2011; Park et al., 1999).

Due to the dispersive properties of Rayleigh waves, wave components with different frequencies penetrate to different depths and provide therefore information about material properties of soil layers at diverse depths (Sólnes, Sigmundsson & Bessason, 2013; Xia et al. 2002). When processing SASW measurements, time series from two geophones are used at a time. For a given site, several measurements must be taken, with varying source offset and possibly by using different types of impact load, in order to excite waves with different frequency contents. Furthermore, the process is repeated from the other end of the geophone lineup, in order to cover possible effects of internal phase shifts due to receivers and instrumentation (Park et al., 1997). When surface waves are generated with a load that can be handled by manpower, e.g. a sledgehammer, a reliable estimate of shear wave velocity down to around 20 m depth can be obtained at best surroundings (Bessason & Erlingsson, 2011; Sólnes et al., 2013).

Due to the necessity of repeated measurements with different field deployments, data acquisition in the field is both time and labor consuming. The data processing involved in the SASW method is as well time intensive. Calculations must be repeated for each receiver pair separately and the results for each pair manually examined in order to evaluate the quality of the results. Moreover, as time series from only two receivers are used at a time, difficulties can arise in distinguishing reliable surface wave signal from noise, such as inclusion of body waves and/or higher modes (Park et al., 1997). This may cause errors in the dispersion curve and ultimately in the shear wave velocity profile. As empirical criteria, manually adjusted to each test site, must be used to detect possible noise, the SASW method cannot be fully automated.

The SASW method is generally divided into three steps; *field measurements*, *data processing* and *inversion analysis*. Each step is described shortly in Sections 3.1 to 3.3. The inversion analysis involved in the SASW method is analogous to the inversion analysis of the MASW method. A general overview of inversion procedures is given in Chapter 7.

3.1   Field measurements

Geophones are lined up in a straight line on the surface of the test site and connected to a data acquisition card and a computer equipped with the necessary software. The number of geophones is typically between two and twelve. The geophones are either planted with equal spacing (see Figure 3.1) or, as is more common, with varying spacing, though in a symmetrical lineup (see Figure 3.2). The distance between individual geophones, and therefore the length of the profile, depends on the intended depth of penetration. More distance between geophones makes it possible to detect waves that penetrate deeper. A shorter profile results in a shallower sampling (Bessason & Erlingsson, 2011; Kaldal, 2007).
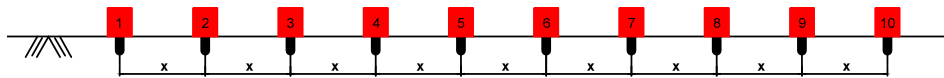
Figure 3.1: Example of a SASW measurement profile. Lineup of ten geophones with equal spacing.
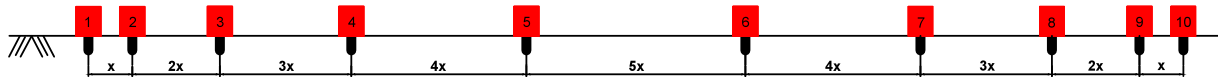
Figure 3.2: Example of a SASW measurement profile. Symmetrical lineup of ten geophones with unequal spacing.

A wave is generated with an impact load at one end of the lineup and the geophones record the vertical component of the resulting wave motion as a function of time. The process is repeated with different types of impact load and different source offsets to sample the desired frequency range. Furthermore, the process is repeated from the other end of the sensor lineup (Bessason & Erlingsson, 2011; Sólnes et al., 2013).

3.2   Data processing

The recorded time histories are analyzed in the frequency domain, resulting in an experimental dispersion curve for the test site. The following description of data processing procedures to extract fundamental mode dispersion curves from recorded data is mainly based on Bessason and Erlingsson (2011) and Kaldal (2007).

When processing SASW measurements, time series from two geophones are used at a

time. The two geophones are referred to as sensor j and sensor k and the recorded time series are denoted by $u_j(t)$ and $u_k(t)$. The sensor pairs are chosen in a way that the distance from the source point to the sensor that is closer to the source point (d_L) is equal or very similar to the distance between the two sensors (d_{jk}) as indicated in Figure 4.1.
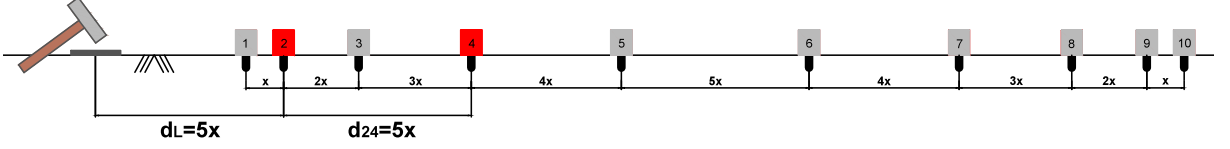
Figure 3.3: SASW data processing. Time series from two geophones are used at a time. The distance from the source point to the sensor that is closer to the source point (d_L) must be the same or similar to the distance between the two sensors (d_{jk}).

The cross-spectral density $(P_{jk}(f))$ of each pair of time series is computed (Bessason & Erlingsson, 2011). The cross-spectral density gives the distribution of the power of the recorded waves per unit frequency, and makes it therefore possible to determine the relationship between the two time series as a function of frequency (Stoica & Moses, 2005).

Before determining the cross-spectral density, the measured time series are transformed into functions of frequency using a Fourier transform (Kaldal, 2007).

$$u_j(t) \xrightarrow{\mathcal{F}} \tilde{u}_j(f) \tag{3.2.1}$$

$$u_k(t) \xrightarrow{\mathcal{F}} \tilde{u}_k(f) \tag{3.2.2}$$

The cross-spectral density of the two time series is then defined as:

$$P_{jk}(f) = \tilde{u}_j(f)\overline{\tilde{u}_k(f)} \tag{3.2.3}$$

$P_{jk}(f)$ is a complex valued function of frequency that in polar form is expressed as:

$$P_{jk}(f) = M_{jk}(f)e^{i\theta_{jk}(f)} \tag{3.2.4}$$

where $M_{jk}(f)$ is the magnitude spectrum and $\theta_{jk}(f)$ is the phase spectrum (Kaldal, 2007).

The magnitude spectrum indicates the dominant frequency components that are simultaneously present in $\tilde{u}_j(f)$ and $\tilde{u}_k(f)$. The phase spectrum identifies the relative phase of each of the frequency components present in the two time series (Stoica & Moses, 2005).

The magnitude and phase spectra are by complex analysis determined by Eqs. (3.2.5) and (3.2.6) (Kaldal, 2007):

$$M_{jk}(f) = P_{jk}(f)\overline{P_{jk}(f)} \tag{3.2.5}$$

$$\theta_{jk}(f) = \arctan\left(\frac{\text{Im}(P_{jk}(f))}{\text{Re}(P_{jk}(f))}\right) \tag{3.2.6}$$

13

The travel time of Rayleigh waves between each pair of sensors can be calculated from the phase spectrum according to:

$$t_{jk}(f) = \frac{\theta_{jk}(f)}{2\pi f} \qquad (3.2.7)$$

where $t_{jk}(f)$ is the time it takes a Rayleigh wave component of frequency f to propagate the distance d_{jk} between sensors j and k.

The Rayleigh wave phase velocity at frequency f $(V_{R,jk}(f))$ is then obtained by:

$$V_{R,jk}(f) = \frac{d_{jk}}{t_{jk}(f)} \qquad (3.2.8)$$

The wavelength (λ) is related to the Rayleigh wave phase velocity and the wave component frequency according to:

$$\lambda(f) = \frac{V_{R,jk}(f)}{f} \qquad (3.2.9)$$

Using Eqs. (3.2.7) to (3.2.9) the dispersion curve for sensors j and k, showing $V_{R,jk}$ as a function of wavelength, is obtained (Bessason & Erlingsson, 2011; Kaldal, 2007).

Dispersion curves for different pairs of receivers are determined and thereafter combined. Diverse dispersion curves are added up within 1/3 octave wavelength bands. All values within each band are grouped together and their average used as a estimate of the phase velocity of Rayleigh wave components belonging to the given frequency range. Error bounds for the average dispersion curve can be obtained using the standard deviation of the values within each frequency band (Bessason & Erlingsson, 2011; Kaldal, 2007).

3.3 Inversion analysis

A theoretical dispersion curve for the test site is obtained, with iteration, based on an assumed number and thickness of soil layers and assumed material properties (e.g. shear wave velocity) for each layer. The experimental dispersion curve is used as a reference and the layers and the shear wave velocity profile that result in a theoretical dispersion curve that fits the experimental one are taken as the result of the survey (Bessason & Erlingsson, 2011). A general overview of inversion procedures is provided in Chapter 7.

Chapter 4

Multichannel Analysis of Surface Waves

The *Multichannel Analysis of Surface Waves (MASW)* method was introduced by Park et al. (1999). In general, MASW surveys can be divided into active and passive surveys based on how the surface waves required for analysis are acquired. In the *active MASW method*, surface waves are generated actively by impulsive or vibrating seismic sources whereas the *passive MASW method* utilizes surface waves generated by natural sources or cultural activities, e.g. traffic (Park et al., 2007). The MASW method was developed in order to overcome some of the weaknesses of the SASW method (see Chapter 3). The principal reported advantages of the MASW method are the following:

- Data acquisition in the field is much less time-consuming as compared to the SASW method. The MASW method requires only a single shot gather for one source-receiver configuration. However, if the SASW method is used, it is necessary to record repeated shots for different field deployments to sample the desired frequency range (Park et al., 1999; Xia et al., 2002).

- The dispersion analysis involved in MASW is faster and easier to automate. Data from all receivers is processed at once, instead of repeated calculations for multiple pairs of receivers as in the SASW method (Xia et al., 2002).

- Noise sources can more easily be identified and noise eliminated as compared to the SASW method (Park et al., 1999; Xia et al., 2002). Reduction of noise leads to increased accuracy in the dispersion analysis and ultimately a more precise shear wave velocity profile.

- The MASW technique can provide more investigation depth than the SASW method, given the same impact load. The maximum depth of investigation that can be achieved by using the (active) MASW method is generally around 30 m, assuming that surface waves are generated by a reasonably heavy seismic source, e.g. a sledgehammer (Park et al., 2007). However, the SASW method can provide an estimation of shear wave velocity down to around 20 m depth at best surroundings (Bessason & Erlingsson, 2011). Passive MASW surveys result in more investigation depth than active surveys (Park et al., 2007).

- The MASW method makes it possible to observe multi-modal dispersion characteristics from recorded surface wave data (Park et al., 1998; Xia et al., 2003).

- The MASW method makes it cost- and time-effective to evaluate shear wave velocity in two and/or three dimensions (Park et al., 2007; Xia et al., 2000).

- The MASW method can be used to analyze passively generated surface waves. Surface waves that are generated by passive sources have lower frequencies (longer wavelengths) than waves generated by impact (active) loads. The use of passively generated surface waves can therefore increase the investigation depth substantially (Park et al., 2007).

In this report, the main focus will be on active MASW surveys, producing a one-dimensional shear wave velocity profile. MASW surveys that produce two-dimensional shear wave velocity profiles and passive MASW surveys will be discussed shortly in Sections 4.2 and 4.3, respectively. If not specifically indicated, the term *MASW survey* refers to an active MASW survey resulting in a one-dimensional dispersion curve and therefore a one-dimensional shear wave velocity profile.

4.1   General procedure

MASW surveys can be broken down into three steps; *field measurements*, *data processing* and *inversion analysis* (Park et al., 1999). Field procedures and data processing methods for MASW surveys are described in more detail in Chapters 5 and 6. Inversion analysis is shortly addressed in Chapter 7.

Field measurements

Geophones are lined up in a straight, equally spaced line on the surface of the test site. A wave is generated with an impact load at one end of the lineup and the geophones record the resulting wave motion as a function of time. A single shot gather is sufficient (Park et al., 1999).

Data processing

A dispersion curve is extracted from the measured surface wave data. Two different analysis methods are described. A *swept-frequency approach* (Park et al., 1999) and the *phase-shift method* (Park et al., 1998).

Inversion analysis

A theoretical dispersion curve for the test site is obtained, with iteration, based on an assumed number and thickness of soil layers and assumed material properties, such as shear wave velocity, for each layer. The experimental dispersion curve is used as a reference (Park et al., 1999). The shear wave velocity profile and the layer structure that result in a theoretical dispersion curve that fits the experimental one are taken as the result of the survey.

An overview of the main steps of the MASW method is provided in Figure 4.1.
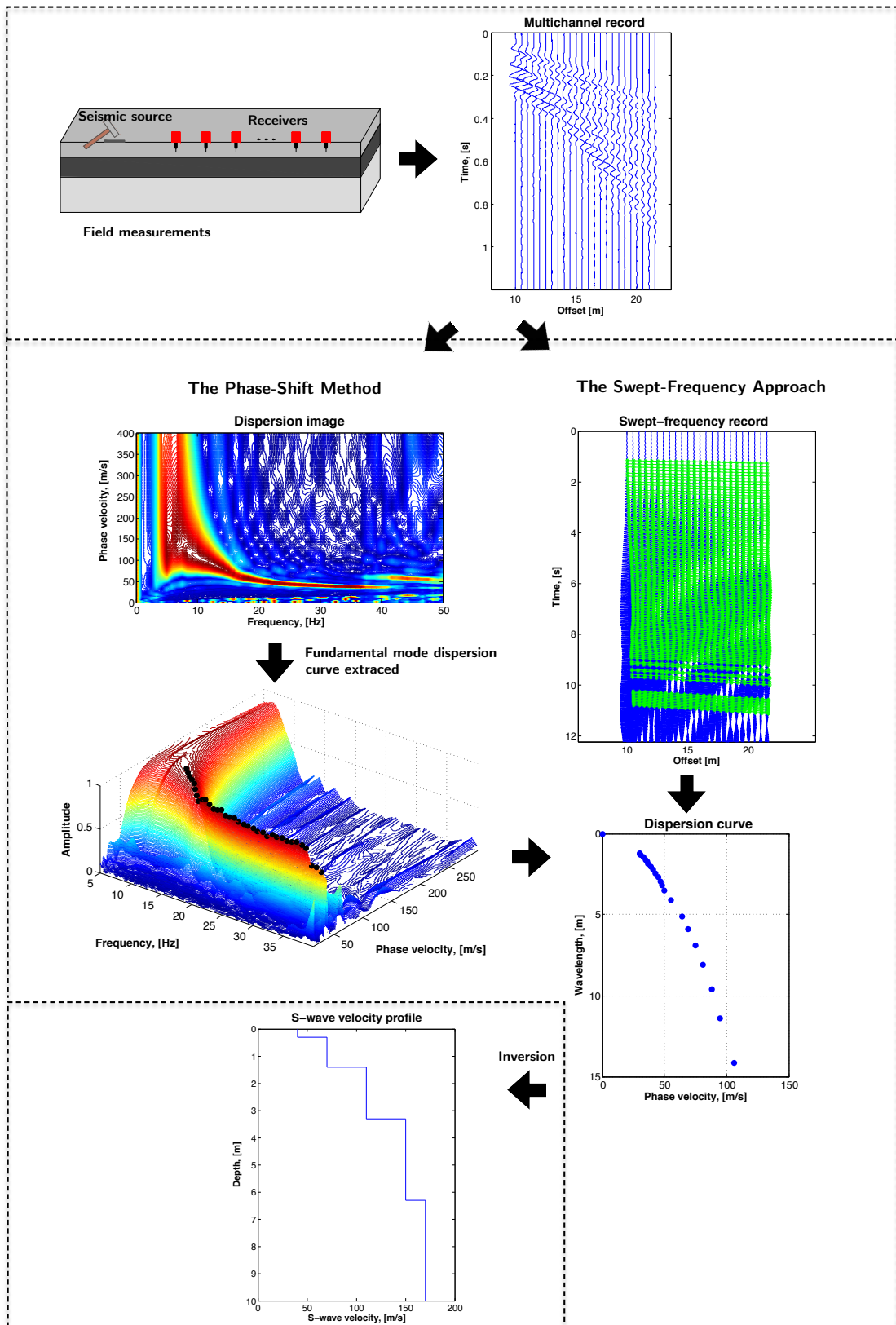
Figure 4.1: Overview over the MASW method.

4.2   2D MASW surveys

Using the MASW technique, a two-dimensional shear wave velocity map, displaying shear wave velocity for a given site as a function of both depth and surface location, can be obtained in a cost-effective and time-effective way (Park et al., 2007; Xia et al., 2000). The main advantage of a two-dimensional profile is increased accuracy, as a two-dimensional profile makes it possible to detect lateral variations of subsurface material properties (Xia et al., 2000).

To obtain a two-dimensional profile, surface wave data is collected for multiple field deployments as the source and geophones roll along the survey line (Xia et al., 2000). Generally, data acquisition is done by the use of a land streamer (an array of geophones connected to a seismic cable that is designed to be towed along the ground) that is attached to a vehicle (MASW, n.d.a.). A dispersion curve is obtained for each record, e.g. by using the data processing procedures described in Chapter 6, and subsequently inverted to obtain a one-dimensional shear wave velocity profile. Each profile is assumed to be representative of the soil deposit directly below the center of the receiver array at the time of the corresponding measurement. A two-dimensional shear wave velocity map is then obtained by interpolation between the various one-dimensional profiles (Xia et al., 2000).

4.3   Passive MASW surveys

Passive MASW surveys utilize passively generated surface waves, i.e. surface waves generated by natural sources or cultural activities, e.g. traffic. Passively generated surface waves are usually of relatively low frequency (1-30 Hz) and with wavelengths ranging from several tens of meters to few kilometres. The investigation depth in passive surveys can therefore reach several hundred meters, whereas it is usually less than 30 m in active surveys (Park et al., 2007).

Passive MASW surveys are divided into two categories; *passive remote* and *passive roadside surveys*. In passive remote MASW surveys, a two-dimensional receiver array of a fairly symmetric shape, e.g. a cross or a circle, is used to record passively generated surface waves. Passive remote MASW surveys result in an accurate one-dimensional shear-wave velocity profile. This method is therefore suitable if one-dimensional shear-wave velocity profiling is needed for a relatively limited area. In passive roadside MASW surveys, receivers are normally lined up in a straight line along a shoulder of a road or a sidewalk and surface waves generated by local traffic are utilized for analysis. The resulting shear wave velocity profile is generally two-dimensional with a surface distance determined by the survey length (Park et al., 2007).

Results from active and passive MASW surveys can be combined, generally by merging of dispersion images. The lower frequency-range of the resulting phase velocity spectra is obtained from passively generated surface waves, while the higher frequency-range is

obtained by an active survey. The main advantages of combined surveys are enlarged investigation depth range and the possibility of improved modal identification (Park et al., 2007).

Chapter 5

Field measurements

This chapter describes the field parameters that are generally recommended for MASW surveys. Emphasis is on recording of surface waves that are produced by an impulsive seismic source. Additional parameters recommended for swept-frequency records are addressed in Section 6.1.

For data acquisition, geophones are lined up in a straight line on the surface of the test site. As the geophones only record vertical motion, it is important that they are placed vertically on the ground. The geophones are connected to a data acquisition card and a computer equipped with the necessary software. Low-frequency geophones (e.g. 4.5 Hz) are recommended (MASW, n.d.a.).

The number of geophones used is usually twelve or more, each connected to a separate recording channel (Park et al., 1997). In reported surveys, a common number of geophones used is 24 and 48 (e.g. Donohue, Dermot & Donohue, 2013; Lin, Chang & Lin, 2004; Park & Carnevale, 2010). Generally, by increasing the number of geophones used for recording, a higher resolution in the dispersion image can be obtained (Park et al., 2001; Ryden, Park, Ulriksen & Miller, 2004). The receivers should be lined up with equal spacing (Park et al., 1997). A general measurement profile for an active MASW survey with 24 geophones is shown in Figure 5.1.
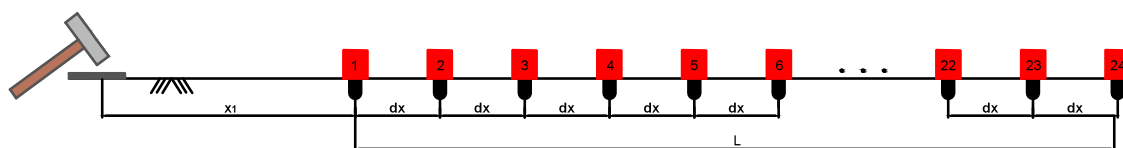
Figure 5.1: Example of a MASW measurement profile. Lineup of 24 geophones with equal spacing (dx). The source offset is x_1.

A recording frequency (f_s) of 1000 Hz is most commonly used in MASW surveys. This corresponds to a sampling interval (dt) of 1 ms. For MASW surveys utilizing an impulsive seismic source, the total recording time (T) is usually around 1 second. A longer recording time (e.g. T = 2 seconds) is recommended for a long receiver spread, i.e. L > 100 m, or if very low shear wave velocities, i.e. $V_s < 100$ m/s, are expected (MASW, n.d.a.). For directly obtained swept-frequency records, i.e. surface wave records generated by a vibrating seismic source, a longer recording time is required (Park et al., 1999) (see Section 6.1).

The maximum depth of investigation (z_{max}) will vary with site and type of seismic source used. The maximum investigation depth is determined by the longest surface wave wavelength that is obtained during data acquisition (λ_{max}). A commonly adopted empirical criteria (Park & Carnavele, 2010) is that:

$$z_{max} \approx 0.5\lambda_{max} \tag{5.0.1}$$

In general, a heavier seismic source will result in increased investigation depth. A common choice is a reasonably heavy sledgehammer (e.g. 10 kg) that can result in an investigation depth of 10-30 m. A source that is capable of delivering more impact power into the ground, such as a crane and a heavy falling load, has potentials to create surface waves of lower frequencies (longer wavelengths), therefore increasing the investigation depth below 30 m. The use of an impact plate (base plate), either metallic or non-metallic, can in addition help generating lower frequency surface waves. A metallic plate is a more conventional choice. However, it has been reported that it is possible to generate surface waves containing noticeable lower frequencies by using a firm rubber plate (MASW, n.d.a.).

The length of the receiver spread (L) is related to the longest wavelength that can be analyzed and therefore also related to the maximum depth of investigation. A common criteria is that the maximum wavelength that can be analysed, with highest possible accuracy, is approximately equal to the length of the receiver spread (Park & Carnevale, 2010):

$$\lambda_{max} \approx L \tag{5.0.2}$$

Attempts to analyze longer wavelengths than indicated by Eq. (5.0.2) will risk less accurate results. Recent studies have shown that the fluctuating inaccuracy will although be within 5% for the interval $L \leq \lambda_{max} \leq 2L$ (Park & Carnevale, 2010).

Utilizing Eq. (5.0.2), the previously presented empirical criteria regarding maximum depth of investigation, Eq. (5.0.1), can be written in terms of the length of the receiver spread as:

$$z_{max} \approx 0.5L \tag{5.0.3}$$

Thus, the optimum receiver spread length has been suggested to lie within the range of (MASW, n.d.a):

$$z_{max} \leq L \leq 3z_{max} \tag{5.0.4}$$

In practice, a very long receiver spread should though be avoided. Surface waves generated by most common seismic sources will have become attenuated below noise level at the end of an excessively long receiver spread, making the signal from the furthermost receivers too noisy to be usable (MASW, n.d.a.; Park et al., 1999).

The receiver spacing (dx) is related to the shortest wavelength that can be analyzed, thus determining the shallowest resolvable depth of investigation (z_{min}) (MASW, n.d.a.), i.e.

$$dx = n \cdot z_{min} \qquad \text{where} \qquad 0.3 \leq n \leq 1.0 \qquad (5.0.5)$$

The distance between the source and the nearest receiver is commonly referred to as the source offset, denoted by x_1. By optimizing the source offset, for a given measurement profile, undesirable near-field effects, such as the risk of not fully developed surface waves being picked up by the geophones, can be minimized. Near-field effects have the tendency to lead to underestimated phase velocities and decreased investigation depth in MASW surveys (Park & Carnavare, 2010).

The minimum source offset required to avoid undesirable near-field effects depends on the longest wavelength being analyzed (λ_{max}). A commonly recommended criteria for MASW surveys is (Park & Carnavare, 2010; Park et al., 1999):

$$x_1 \geq 0.5L \qquad \text{where} \qquad \lambda_{max} \approx L \qquad (5.0.6)$$

It has been reported that a long source offset, i.e. $x_1 \geq L$, could enhance energy for long-wavelength surface waves, thus increasing λ_{max} for a given receiver spread (Park & Carnavare, 2010). However, such a long source offset can result in lack of short-wavelength wave components due to excessive attenuation (Park & Shawver, 2009). A suggested minimum and maximum source offsets have been reported as (MASW, n.d.a.):

$$x_{1,min} = 0.2L \qquad \text{and} \qquad x_{1,max} = L \qquad (5.0.7)$$

Apart from various data acquisition parameters, topographical conditions are known to have effect on the quality of the recorded surface wave data and therefore the quality of the resulting dispersion curves. For optimum results, the receivers should be placed on a relatively flat terrain. (See Figures 5.2 (a) and (b).) Especially, surface reliefs within the receiver span greater than around $0.1L$ can have significant effect on the generation of surface waves (MASW, n.d.a.). (See Figure 5.2 (c).)

The slope of the surface along the receiver span can as well affect the accuracy of the resulting dispersion curves. Results of numerical investigations presented by Zeng et al. (2012) displayed that dispersion characteristics can be estimated with less than 4% error where the slope of the topography along the receiver span is less than 10°.
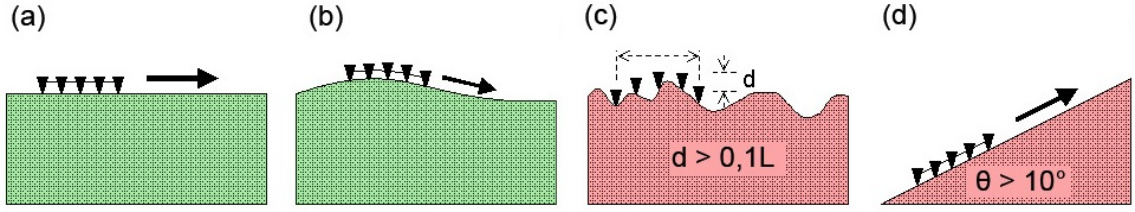
Figure 5.2: Topographical conditions are found to have effect on the quality of the recorded multichannel surface wave data. Receivers should be placed along a relatively flat ground for optimum results (figures (a) and (b)). Surface reliefs greater than $0.1L$ and slope more than 10° are reported to have significant effect on the quality of the recorded data (figures (c) and (d)). Based on MASW (n.d.a).

Table 5.1 summarizes several field parameters related to data acquisition for active MASW surveys as indicated by Eqs. (5.0.2), (5.0.3) and (5.0.6). The length of the receiver spread (L) and the source offset (x_1) are given within a range as indicated by Eqs. (5.0.4) and (5.0.7), respectively. The receiver spacing (dx) is calculated assuming that 24 receivers are used for data acquisition. Possible effects of surface wave attenuation (i.e. due to the length of the receiver spread or the source offset) are not specifically considered in Table 5.1.

The values listed in Table 5.1 should be taken as guidelines and a rather large tolerance in all parameters might be expected (at least $\pm$ 20% as suggested in MASW (n.d.a)).

Table 5.1: Summary of field parameters related to data acquisition for active MASW surveys. The values should be taken as guidelines.

Depth z_{max} [m]	Maximum wavelength λ_{max} [m]	Length of receiver spread L [m]	Source offset x_1 [m]	Receiver spacing (24-channel) dx [m]
		(5-15)	(1-15)	(0.2-0.7)
5	10	10	5	0.4
		(10-30)	(2-30)	(0.4-1.3)
10	20	20	10	0.9
		(20-60)	(4-60)	(0.9-2.6)
20	40	40	20[*]	1.7
		(30-90)	(6-90)	(1.3-3.9)
30	60	60	30[*]	2.6

[*] It has been reported (Park, Miller & Miura, 2002) that a source offset of 10 m will be enough to assure plane wave propagation for waves with wavelengths up to 60 m.

Chapter 6

Dispersion analysis

Accurate construction of dispersion curves has been described as the most critical part of a MASW analysis (Park et al., 1997). Several methods to extract dispersion curves from recorded multichannel surface wave data have been developed (e.g. McMechan & Yedlin, 1981; Park et al., 1998; 1999). Two different approaches will be discussed in this chapter. They are:

1. Multichannel analysis using a *swept-frequency approach* (Park et al., 1999).

2. The *phase-shift method* (also known as the *wavefield transformation method*) (Park et al., 1998).

6.1 Swept-frequency approach

The swept-frequency approach to extract fundamental mode dispersion curves from multichannel surface wave data was first described by Park et al. (1999). The basis of the method is the trace-to-trace coherency in amplitude and arrival time of surface waves that is observed on multichannel records. By displaying the multichannel record in a swept-frequency format, the Rayleigh wave phase velocity at different frequencies can be determined. Due to the linear separation of each ground roll frequency component, the phase velocities are obtained by calculating the linear slope of each frequency component (Park et al., 1999).

On swept-frequency records, noise sources, e.g. body waves and higher mode surface waves, are generally observed as breaks in the otherwise coherent surface wave motion. As only minor data processing is required to obtain a swept-frequency record from an impulsive shot gather (and no data processing required if a vibrating seismic source is used), noisy data can be identified in situ with minimal effort. Thus, swept-frequency records permit effective reduction of noise by possible adjustments of recording and/or field setup parameters, e.g. source-receiver offset, during data acquisition (Park et al., 1999).

The method can be divided into two steps:

1. Obtaining a swept-frequency record.

2. Calculating the Rayleigh wave phase velocity as a function of frequency from the linear slopes of each component of the swept-frequency record.

The main data processing steps are shown schematically in Figure 6.1 followed by a brief description of each step. A more detailed description of the method follows in Sections 6.1.1 and 6.1.2.

1. Swept-frequency record

①   (a) Indirect recording of $u_s(x, t)$.

$$Impulsive\ record\ \xrightarrow[\text{a stretch function}]{\text{convolution with}}\ Swept\text{-}frequency\ record$$

or

(b) Direct recording of $u_s(x, t)$.

2. Dispersion curve from a swept-frequency record

②   Identify and extract linear events $(u_{lin,l})$.

③   Determine the frequency corresponding to each linear event (f_l).

④   Regression $\longrightarrow$ Linear slope of each linear event (a_l).

⑤   Calculate Rayleigh wave velocity as a function of frequency.
$$V_{R,l} = a_l^{-1}\ at\ f = f_l$$
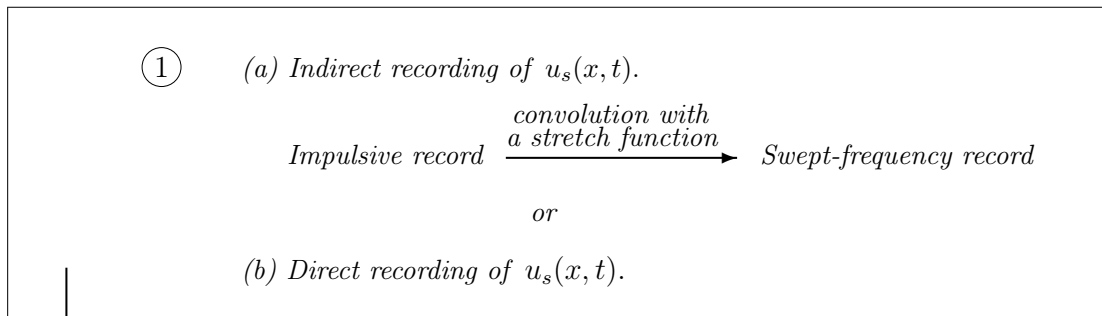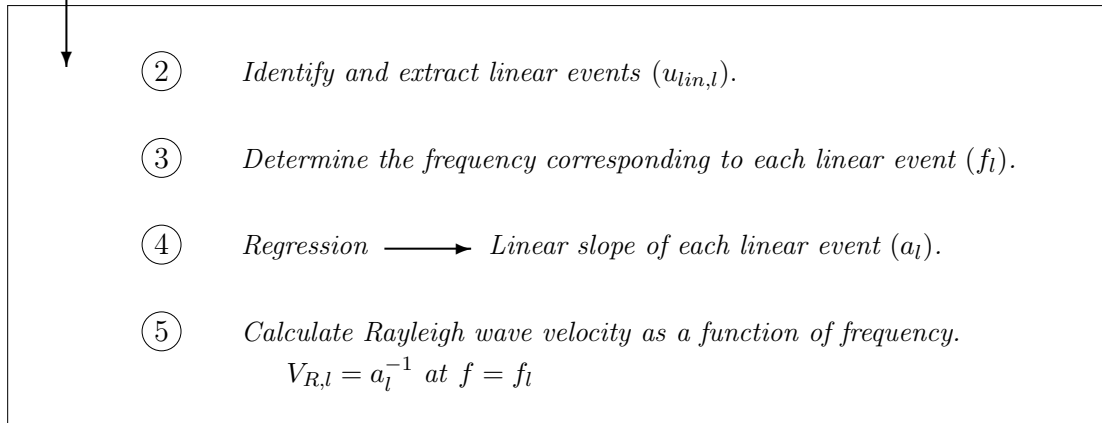
Figure 6.1: An overview of the swept-frequency approach.

The steps listed in Figure 6.1 are the following (Park et al., 1999):

1. A swept-frequency record $(u_s(x, t))$ is obtained by (a) indirect or (b) direct recording. The number of receivers is n. Direct records are obtained by using a vibrating seismic source. For indirect records, a shot gather obtained by an impulsive source is transformed into a swept-frequency record by convolution with a stretch function.

2. Linear events within the swept-frequency record are identified and extracted by examining the trace-to-trace coherency in amplitude and arrival time of the surface waves recorded by each of the n receivers.

3. The frequency corresponding to each linear event is determined. The frequency corresponding to linear event l (f_l) is assumed to be the average frequency within the event.

4. The linear slope of each linear event is determined by using the method of least squares.

5. The Rayleigh wave velocity at the frequency representative of each linear event is determined. The Rayleigh wave velocity is taken as one divided by the slope of the least squares regression line.

6.1.1 Swept-frequency record

A swept-frequency record can either be obtained directly, i.e. by using a vibrating source to obtain swept surface wave data, or indirectly by transforming an impulsive record by convolution with a stretch function (Park et al., 1999).

In signal processing, the way a system responds to a unit impulse is called the impulse response of the system. As the impulse response has been determined, the system's response to any other stimulus can be predicted by the use of convolution. Convolution is a mathematical operation that is used to combine two signals (the input signal and the impulse response) to form a third signal (the output signal). The output signal is the resulting system response to the input signal (Schilling & Harris, 2012). Thus, convolution can be used to infer the response of the layered surface wave medium under study to a frequency-varying stimulus, based on its response to an impulsive seismic source.

Data acquisition parameters for swept-frequency records

The following data acquisition parameters are of special importance for swept-frequency records (Park et al., 1999):

- The length of the direct swept-frequency record or the length of the stretch function (for indirect records) (T).

- The lowest frequency recorded (f_1).

- The highest frequency recorded (f_2).

The maximum investigation depth is related to the longest wavelength obtained during data acquisition according to Eq. (5.0.1). Thus, rewriting Eq. (5.0.1) in terms of frequency utilizing Eq. (2.2.1), it can be shown that the maximum investigation depth is determined by the lowest frequency recorded (f_1) (Park et al., 1999), i.e.

$$z_{max} = \frac{V_R(f_1)}{2f_1} \tag{6.1.1}$$

where $V_R(f_1)$ is the Rayleigh wave phase velocity at frequency f_1.

The lowest frequency that can by recorded is most often limited by the natural frequency of the geophones and the type of seismic source that is used. Thus, for increased investigation depth, lower frequency geophones and/or a different type of seismic source, capable of creating lower frequency surface waves, is suggested (Park et al., 1999).

It is recommended that the highest frequency (f_2) is initially chosen several times higher than considered necessary for analyzes, i.e. several times higher than the expected maximum ground roll frequency. After noise analysis f_2 can be lowered if required (Park et al., 1999).

A long swept-frequency record is recommended, as a longer record allows more detailed examination of changes in ground-roll frequency. A long record is especially vital on sites where near-surface properties are likely to change rapidly with depth. For most sites, $T = 10$ s is sufficient (Park et al., 1999).

Other field parameters, such as receiver spread length (L) and source offset (x_1), are recommended to be chosen as described in Chapter 5.

Stretch function

An impulsive record $u(x, t)$ can be transformed into a swept-frequency record $u_s(x, t)$ by convolution with a stretch function (Park et al., 1999):

$$u_s(x, t) = u(x, t) * s(t) \tag{6.1.2}$$

The convolution operation is applied to each of the n traces of the impulsive record separately, that is:

$$u_{s,j}(t) = u_j(t) * s(t) \qquad j = 1, 2, \ldots, n \tag{6.1.3}$$

$u_{s,j}(t)$: j-th trace of the resulting swept-frequency record $u_s(x, t)$
$u_j(t)$: j-th trace of the impulsive record $u(x, t)$
$s(t)$:   Stretch function given by Eq. (6.1.5)

The linear convolution operator is denoted by $*$. The linear convolution of $u_j(t)$ and $s(t)$ is computed according to:

$$u_j(t) * s(t) = \sum_{i=0}^{t} u_j(t - i)s(t) \qquad t \geq 0 \tag{6.1.4}$$

The stretch function is a sinusoidal function with changing frequency as a function of time. A suggested choice is a linear sweep with frequency varying from f_1 to f_2 (Park et al., 1999):

$$s(t) = \sin\left(2\pi f_1 t + \frac{\pi(f_2 - f_1)}{T}t^2\right) \tag{6.1.5}$$

where f_1 and f_2 are the lowest and highest frequencies to be analyzed and T is the length of the stretch function.

Using the computational software Matlab, the built-in function `conv` (Schilling & Harris, 2012) can be used to convolve the measured time signal and the stretch function. Each trace must be convolved with the stretch function separately as suggested by Eq. (6.1.3).

Figure 6.2 shows an example of a convolution of a single trace from an arbitrary impulsive shot gather (Figure 6.2 (middle)) with a stretch function. The length of the stretch function in the figure is T = 1.2 s, with linearly changing frequency from $f_1 = 5$ Hz to $f_2 = 30$ Hz. The resulting swept-frequency trace is shown in Figure 6.2 (bottom).
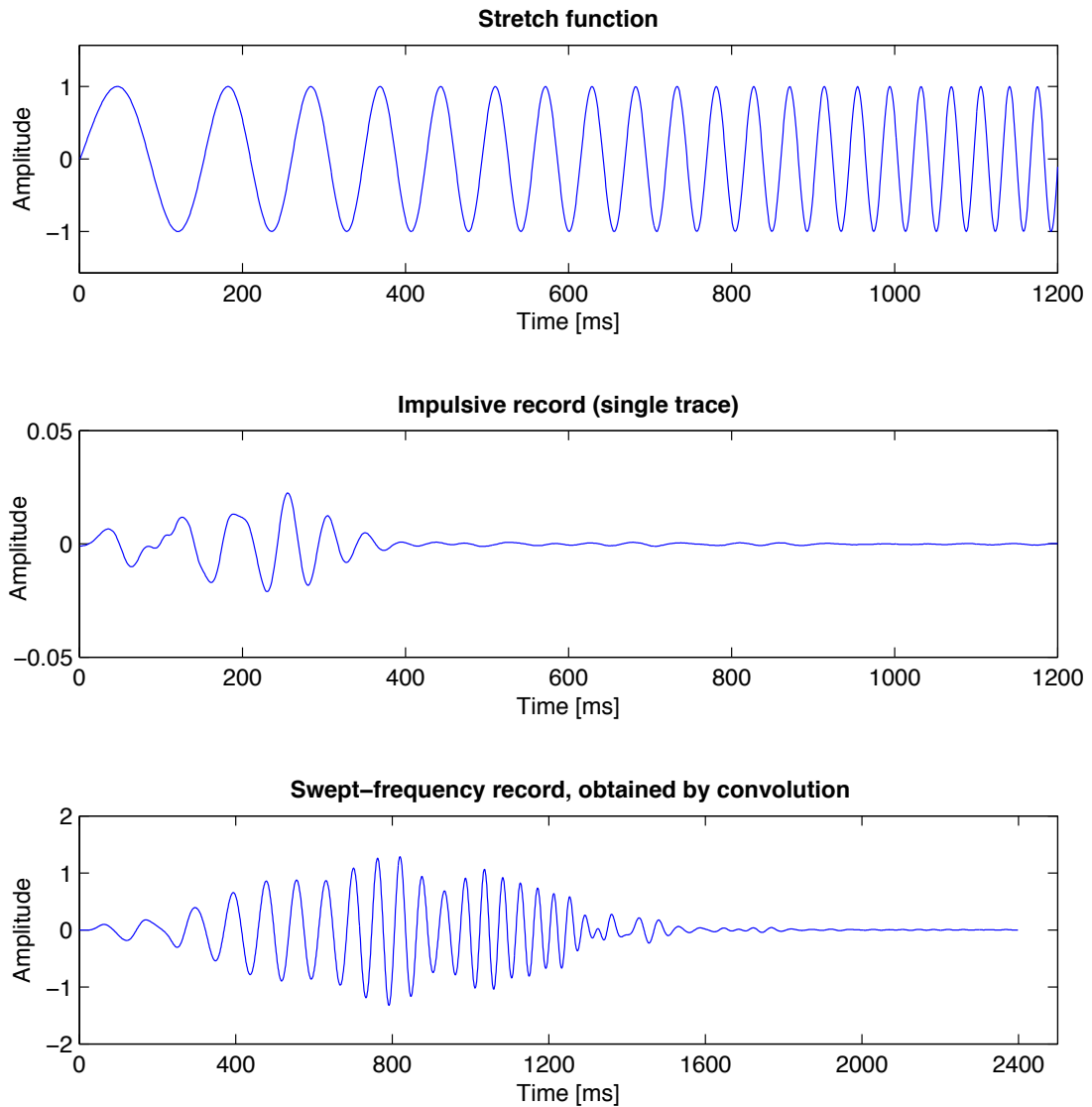

Figure 6.2: Example of convolution of a single trace from an impulsive shot gather with a stretch function. Top: Stretch function with linearly changing frequency from $f_1 = 5$ Hz to $f_2 = 30$ Hz. Middle: Recorded data. Bottom: Resulting swept-frequency trace obtained by convolution.

6.1.2   Dispersion curve from a swept-frequency record

Rayleigh wave phase velocity is calculated from the linear slope of each frequency component within the swept-frequency record. The linear ground-roll coherency of a frequency component within the swept-frequency record is referred to as a *linear event* (Xia et al., 2002).

Only those parts of the swept-frequency record where the linear events are undisturbed can be used for further analysis. On multichannel swept-frequency records, the presence of near-field effects is often evident by lack of ground-roll coherency in the low-frequency part of the record. Far-field effects, e.g. attenuation of ground-roll and contamination by body waves, are likewise often apparent in the high-frequency part of the record. On a record displayed in swept-frequency format, far-field effects can generally be identified by decrease in slope of linear events with frequency and/or decline in linear coherency at high frequencies. Far-field effects are in general initially apparent at the far-offset traces, but become also evident at near-offset traces with increasing frequency. Near-field and far-field effects can be minimized by careful chose of data acquisition parameters and proper test configuration (see Chapters 5 and 6.1.1) (Park et al., 1999).

Computational method

This section describes a computational method to determine a fundamental mode Rayleigh wave dispersion curve based on a swept-frequency record. The algorithm was developed using the computational software Matlab. The main disadvantage of this approach is that the computations have not yet been fully automated. Further testing is needed to verify the approach.

Each trace of the swept-frequency record is treated as a discrete function of time, denoted by $u_{s,j}(t)$ for receiver $j = 1, 2, \ldots, n$. Figure 6.3 shows an arbitrary 2.4 s long swept-frequency record obtained from an impulsive shot gather by convolution with a stretch function. The record shown in Figure 6.3 consists of ten traces ($n = 10$). The stretch function shown in Figure 6.2 (top) was used to linearly separate frequencies in the range of $f_1 = 5$ Hz to $f_2 = 30$ Hz across the impulsive record. This record will be used for general demonstration of the method.
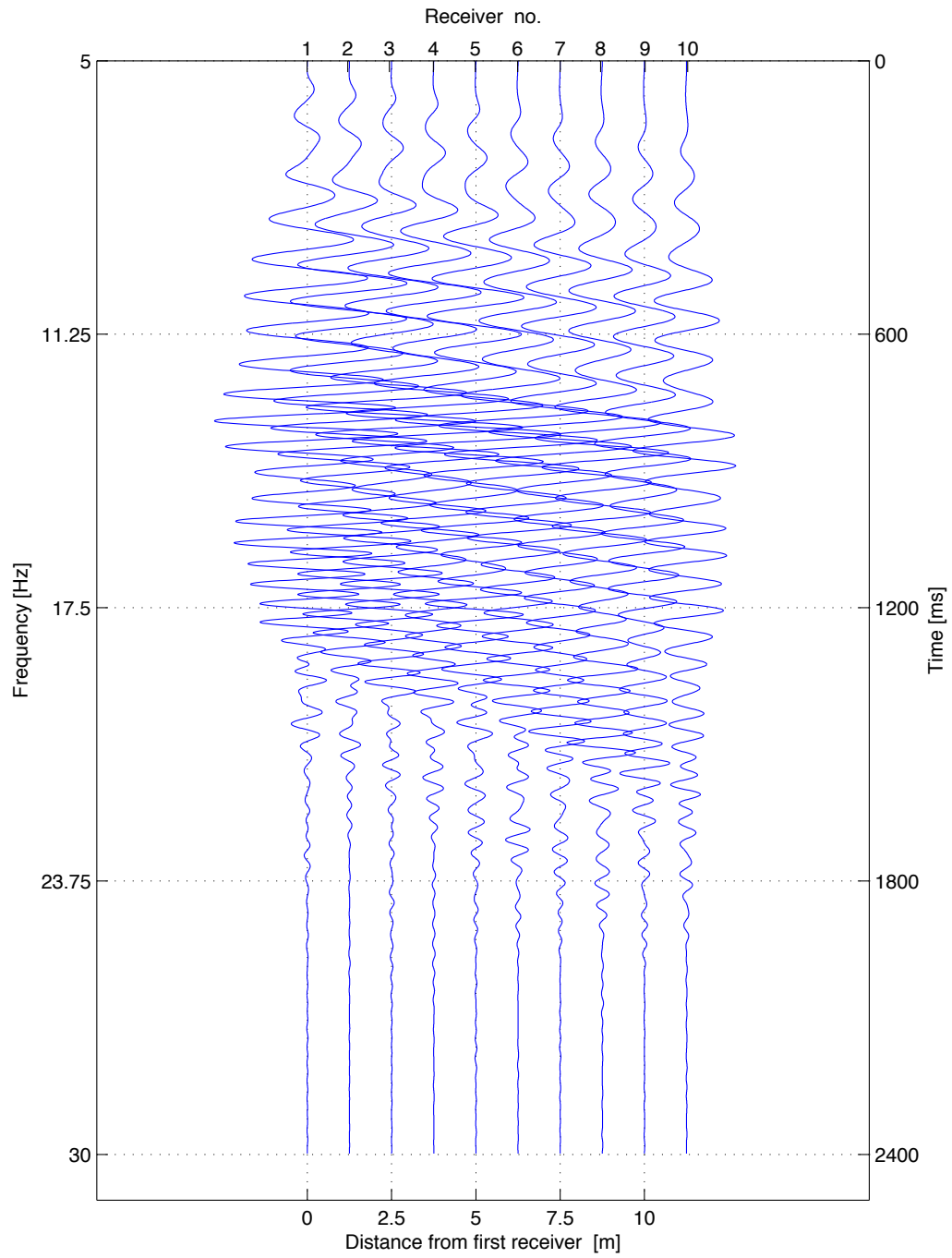
Figure 6.3: Swept-frequency record obtained from an impulsive shot gather by convolution with a stretch function.

The first step consists of finding the local (regional) maxima of each swept-frequency trace, denoted by $u_{s,j}(t_{max,j})$, and the time corresponding to each local maxima $t_{max,j}(k_j)$, $k_j = 1, 2, \ldots, n_{max,j}$ ($n_{max,j}$ is the number of local maxima of trace j). Using Matlab, the local maxima were determined by the built-in function `imregionalmax` (part of the image processing toolbox) (MathWorks, n.d.).

The local maxima that correspond to the lowest and the highest frequencies are excluded due to attenuation/abnormalities that often occur, e.g. because of near-field and far-field effects. The number of values to exclude must to this point be manually customized for each record that is analyzed. Local maxima that are obviously not part of any linear event, i.e. outliers, can as well be excluded from the data at this stage.

Next, linear events are determined. The remaining local maxima of $u_{s,1}(t)$ ($u_{s,1}(t_{max,1})$) are used as a base for the search. The linear events through the data set are denoted by $u_{lin,l}$, $l = 1, 2, \ldots, n_{lin}$ (n_{lin} is the total number of linear events within the record). The array $t_{lin,l}$ contains the time corresponding to each value of $u_{lin,l}$.

An event through the data set is taken as linear and given by Eqs. (6.1.6) and (6.1.7):

$$t_{lin,l} = [t_{max,1}(k_{1,l}) , \; \ldots \; , \; t_{max,n}(k_{n,l})] = [t_{lin,1,l} , \; \ldots \; , \; t_{lin,n,l}] \tag{6.1.6}$$

$$u_{lin,l} = [u_{s,1}(t_{lin,1,l}) , \; \ldots \; , \; u_{s,n}(t_{lin,n,l})] \tag{6.1.7}$$

if Eq. (6.1.8) is fulfilled for all $j \in \{1, 2, \ldots, n-1\}$

$$0 < t_{max,j+1}(k_{j+1,l}) - t_{max,j}(k_{j,l}) < \Delta_{max} \tag{6.1.8}$$

where:
j: Number of receiver.
l: Number of linear event.
$k_{j,l}$:   Number of local maxima, corresponding to receiver j and linear event l.
Δ_{max}: Maximum time lag between two adjacent local maxima within linear event l.

An example is shown in Figure 6.4, using the swept-frequency data presented in Figure 6.3. The local maxima of each swept-frequency trace that fulfill the criteria set by Eqs. (6.1.6) to (6.1.8) are identified by red markers. The local maxima that were excluded from the analysis are shown with blue markers.
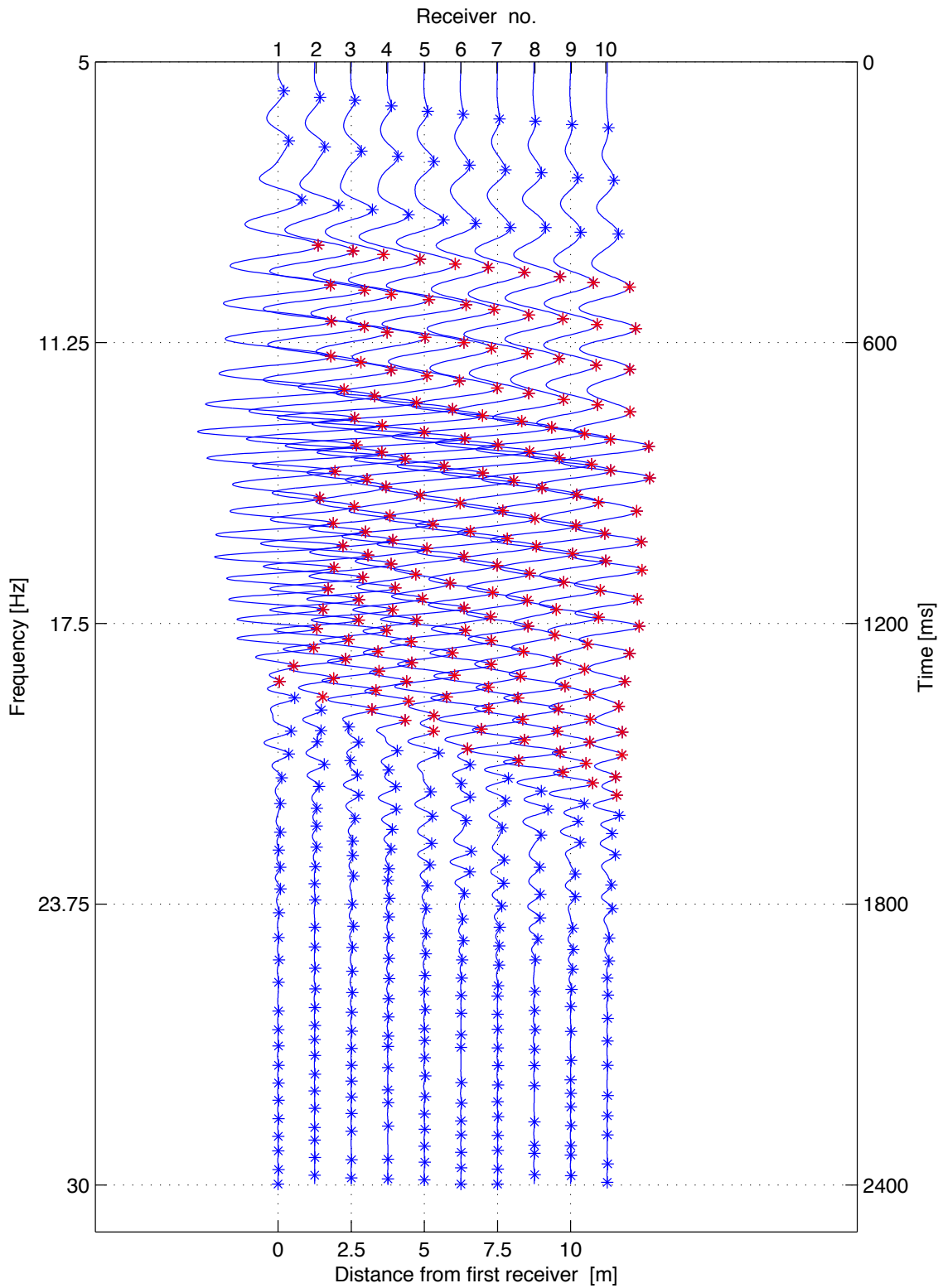
Figure 6.4: Swept-frequency record obtained from an impulsive shot gather. Red markers identify the local maxima of each trace that are parts of linear events that are considered reliable for further analysis. Local maxima that are not used for analysis are shown with blue markers.

Subsequently, linear regression (least squares approach) is used to determine the slope of the best fitting line through each linear event (Bradie, 2006). The slope of linear event l is determined by using the time values corresponding to the local maxima of the event ($t_{lin,l}$) and the surface location of the n geophones used for recording as given by:

$$x_j = (j-1)dx \qquad j = 1, 2, \ldots, n \tag{6.1.9}$$

where dx is the receiver spacing and j is the number of the receiver in the geophone lineup.

The Rayleigh wave phase velocity at the frequency representative of linear event l is taken as one divided by the slope of the least squares regression line. Thus, the phase velocity at frequency f_l ($V_{R,l}$) is obtained according to:

$$\frac{1}{V_{R,l}} = \frac{n \sum_{j=1}^{n} x_j t_{lin,j,l} - (\sum_{j=1}^{n} x_j)(\sum_{j=1}^{n} t_{lin,j,l})}{n(\sum_{j=1}^{n} x_j^2) - (\sum_{j=1}^{n} x_j)^2} \tag{6.1.10}$$

The frequency corresponding to linear event l (f_l) is assumed to be the average frequency within the event, i.e.

$$f_l = \bar{f}_l = f_1 + \frac{t_{avr,l}}{T}(f_2 - f_1) \tag{6.1.11}$$

where

$$t_{avr,l} = \frac{t_{lin,1,l} + t_{lin,n,l}}{2} \tag{6.1.12}$$

$t_{lin,j,l}$: Time of maxima j within linear event l.
x_j: Surface location of receiver j (given by Eq. (6.1.9)).
f_1:   Lowest frequency analyzed.
f_2:   Highest frequency analyzed.
T: Length of swept-frequency record.
n: Number of receivers used for data acquisition.

Figure 6.5 shows an example of two extracted linear events from the swept surface wave data in Figure 6.3. The Rayleigh wave phase velocity and the frequency corresponding to each event, obtained according to Eqs. (6.1.10), (6.1.11) and (6.1.12), are indicated in the figure.
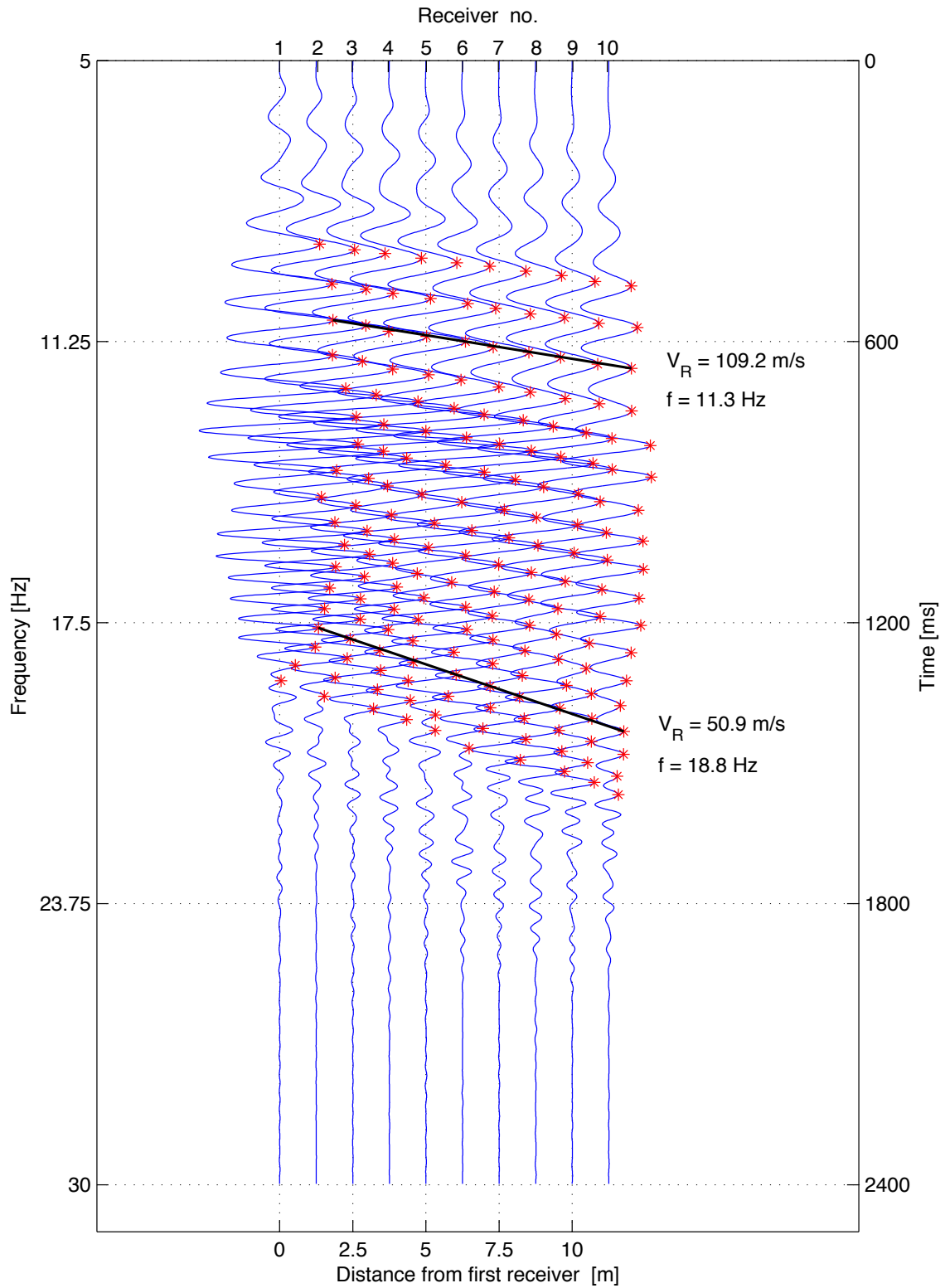
Figure 6.5: Linear events extracted from a swept-frequency record. Red markers identify the local maxima of each trace that are used for identification of linear events. Two linear events, corresponding to frequencies (*f*) of 11.3 Hz and 18.8 Hz are indicated by black lines.

The relations between Rayleigh wave phase velocity and frequency, the dispersion characteristics of the Rayleigh wave, are generally visualized by a dispersion curve. The dispersion curve is by convention presented as a function of phase velocity and wavelength. The transformation from frequency to wavelength is performed according to Eq. (2.2.1). The dispersion curve that was extracted from the swept-frequency record in Figure 6.5 is shown in Figure 6.6. The points corresponding to the marked linear events in Figure 6.5 are specially indicated by red markers in Figure 6.6.
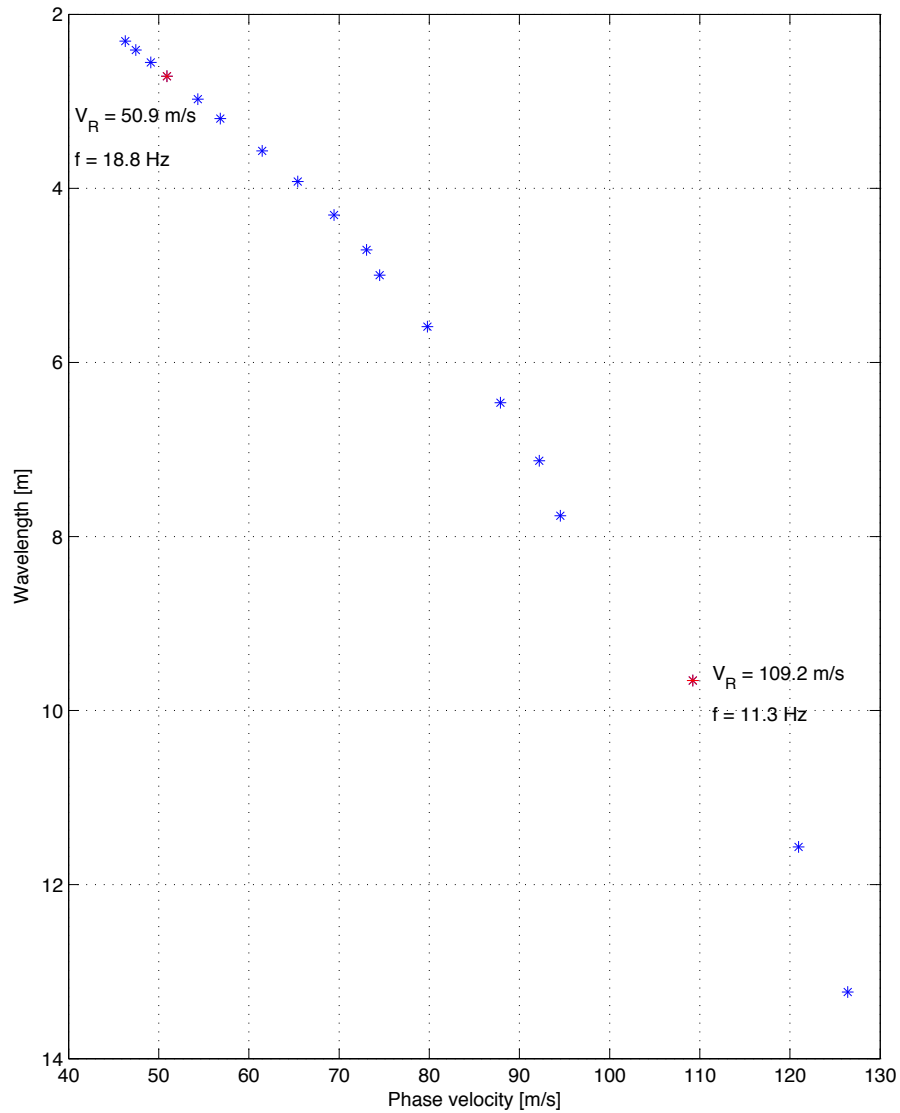
Figure 6.6: Dispersion curve obtained by the swept-frequency approach. Points corresponding to the marked linear events in Figure 6.5 are indicated by red markers.

To increase the resolution of the extracted dispersion curve, it is possible to repeat the process described in this chapter, using the local minima of each swept-frequency trace as references instead of the local maxima, thereby doubling the number of data points obtained.

6.2   Phase-shift method

The *phase-shift method* (also known as the *wavefield transformation method*) was first described by Park et al. in 1998. The phase-shift method is a wave transformation technique to obtain a phase-velocity spectra (dispersion image) based on a multichannel impulsive shot gather (Park et al., 1998).

Using the phase-shift method, the dispersion properties of all types of waves (body and surface waves) contained in the recorded data are visualized in the frequency - phase velocity - transformed energy (summed wave amplitude) domain. Different modes of surface waves are recognized by their frequency content and characterizing phase velocity at each frequency. Noise sources, i.e. body waves and reflected/scattered waves, are likewise recognized by their frequency content and moveout across the receiver array. The required Rayleigh wave dispersion curves are extracted from the dispersion image for further analysis. Noise is usually automatically removed in this process (Park et al., 2007).

This efficient decomposition of the recorded data into different surface wave modes and various noise sources is a great advantage of the phase-shift method. Apart from automatic noise removal, it becomes possible to observe multi-modal surface wave dispersion characteristics, provided that higher modes were excited during data acquisition (Park et al., 1998; Xia et al., 2003).

The phase-shift method can be divided into three steps:

1. Fourier transformation and amplitude normalization.

2. Dispersion imaging.

3. Extraction of dispersion curves.

The most vital data processing steps are shown schematically in Figure 6.7, followed by a brief description of each step. A more detailed description of the phase-shift method follows in Sections 6.2.1 to 6.2.3.

1. Fourier transformation and amplitude normalization

$$
\textcircled{1} \qquad u_j(t) \xrightarrow{\ FFT\ } \tilde{u}_j(\omega) \qquad j = 1, 2, 3, \ldots, n
$$

$$
\textcircled{2} \qquad \tilde{u}_{j,norm}(\omega) = \frac{\tilde{u}_j(\omega)}{|\tilde{u}_j(\omega)|} = P_j(\omega)
$$

2. Dispersion imaging

$$
\textcircled{3} \qquad V_{R,t} : \textit{Testing Rayleigh wave phase velocity}
$$
$$
V_{R,t,min} \leq V_{R,t} \leq V_{R,t,max}
$$

$$
\textcircled{4} \qquad \phi x_j\text{: } \textit{Phase shifts corresponding to a given set of } \omega \textit{ and } V_{R,T}
$$
$$
\phi x_j = \frac{\omega x_j}{V_{R,T}} = \frac{\omega(x_1 + (j-1)dx)}{V_{R,T}}
$$

$$
\textcircled{5} \qquad A_s(\omega, V_{R,T}) : \textit{Summed amplitude for a given set of } \omega \textit{ and } V_{R,T}
$$
$$
A_s(\omega, V_{R,T}) = e^{-i\phi x_1}\tilde{u}_{1,norm}(\omega) + \ldots + e^{-i\phi x_n}\tilde{u}_{n,norm}(\omega)
$$

$$
\textcircled{6} \qquad \textit{Repeat } \textcircled{4} \textit{ and } \textcircled{5} \textit{ for varying } \omega \textit{ and } V_{R,T}
$$

3. Extraction of dispersion curves

$$
\textcircled{7} \qquad A_s(\omega, V_{R,t}) \xrightarrow{\ \textit{extract peak values}\ } \textit{Rayleigh wave dispersion curve(s)}
$$

Figure 6.7: An overview of the phase-shift method.

The steps listed in Figure 6.7 are the following (MASW, n.d.b; Park et al. 1998; Ryden et al., 2004):

1. A Fast Fourier Transformation (FFT) is applied to an n-channel impulsive shot gather ($u_j(t)$, $j = 1, 2, \ldots, n$), to decompose the record into individual frequency components ($\tilde{u}_j(\omega)$, $j = 1, 2, \ldots, n$).

2. The amplitude of each trace of the record (in the frequency domain) is normalized to obtain $\tilde{u}_{j,norm}(\omega)$. As the phase spectrum of the signal ($P_j(\omega)$) contains all information about its dispersion properties, no significant information is lost.

3. A phase velocity range for testing ($V_{R,T,min} \leq V_{R,T} \leq V_{R,T,max}$) is established.

4. For a given testing phase velocity and a given frequency, the amount of phase shifts required to counterbalance the time delay corresponding to specific offsets are determined.

5. The phase shifts (determined in step 4 for a given testing phase velocity) are applied to distinct traces of the transformed shot gather that are thereafter added to obtain the slant-stack (summed) amplitude corresponding to each set of ω and $V_{R,T}$.

6. Steps 4 and 5 are repeated for all the different frequency components of the transformed shot gather in a scanning manner using varying test phase velocities, i.e. changing $V_{R,T}$ by small increments within the previously specified range.

7. The phase velocity spectra (dispersion image) is obtained by plotting the summed amplitude in the frequency – phase velocity – transformed energy (summed wave amplitude) domain, either in two or three dimensions. The peak values (high-amplitude bands) observed display the dispersion characteristics of the recorded surface waves.

6.2.1   Fourier transformation and amplitude normalization

Assume that a multichannel impulsive record has been obtained as described in Chapter 5. The number of geophones used for recording is n. The recorded wavefield is denoted by $u(x,t)$, where x is distance from source to receiver (transmitter-receiver offset) and t is time. The record $u(x,t)$ consists of n traces, one from each geophone, denoted by $u_j(t), j = 1, 2, \ldots n$. The readings of each geophone are acquired with a uniform sampling interval dt.

The source offset is denoted by x_1 and the receiver spacing is dx. The length of the receiver spread is therefore:

$$L = (n-1)dx \qquad (6.2.1)$$

and the distance from the seismic source to receiver j is:

$$x_j = x_1 + (j-1)dx \qquad j = 1, 2, \ldots, n \qquad (6.2.2)$$

The number of samples recorded per unit time, i.e. the measuring frequency in Hz, is denoted by f_s. In terms of angular frequency (ω_s), the measuring frequency is expressed as:

$$\omega_s = 2\pi f_s \qquad (6.2.3)$$

A Fourier transform is applied to the time axis of the recorded wavefield, resulting in its frequency-domain representation $\tilde{u}(x,\omega)$ where ω is angular frequency (Kreyszig, 2011; Park et al., 1998):

$$\tilde{u}(x,\omega) = \int_{-\infty}^{\infty} u(x,t)e^{-i\omega t}dt \qquad (6.2.4)$$

As the recorded wavefield ($u(x,t)$) is discrete in both the space and the time domain, Eq. (6.2.4) describes a one-dimensional discrete Fourier transform (DFT) over time applied repeatedly, i.e. to each trace separately:

$$\tilde{u}_j(\omega_k) = \sum_{m=0}^{N-1} u_j(t_m)e^{-i\omega_k t_m} \qquad (6.2.5)$$

where $j = 1, 2, \ldots, n$ is the number of the corresponding receiver in the geophone lineup. N is the number of components of each data sequence, i.e. the number of sampling points. The total recording time is $T = N dt$ and the sample points are:

$$t_m = m dt \qquad m = 0, 1, \ldots, N - 1 \tag{6.2.6}$$

The frequency sampling points are denoted by ω_k and given as (Schilling & Harris, 2012):

$$\omega_k = \frac{2\pi k}{T} \qquad k = 0, 1, \ldots, N - 1 \tag{6.2.7}$$

For computations, the Fast Fourier Transform (FFT) algorithm is essential. The FFT algorithm accomplishes the DFT of each record with computational complexity of $O(N \log(N))$ instead of $O(N^2)$, as required for direct computations (Kreyszig, 2011; Schilling & Harris, 2012). Using the computational software Matlab, the built-in function `fft`, which computes the discrete Fourier transform of a signal using the Fast Fourier Transform algorithm (Schilling & Harris, 2012), can be utilized to obtain the discrete Fourier transform of each trace $\tilde{u}_j(\omega)$.

In $\tilde{u}(x, \omega)$, the frequency components of the original record $(u(x, t))$ have been separated into individual frequencies as indicated by Eq. (6.2.5). The angular frequency corresponding to component k of the transformed record can be expressed in terms of the sampling frequency as (Schilling & Harris, 2012):

$$\omega_k = k \frac{\omega_s}{N} \tag{6.2.8}$$

where ω_s is the sampling frequency (in radians) given by Eq. (6.2.3) and N is the number of sampling points.

The transformed wavefield $(\tilde{u}(x, \omega))$ can be expressed in terms of the amplitude spectrum $(A(x, \omega))$ and the phase spectrum $(P(x, \omega))$ according to:

$$\tilde{u}(x, \omega) = A(x, \omega) P(x, \omega) \tag{6.2.9}$$

where information about the dispersion properties of the signal is preserved in $P(x, \omega)$ and $A(x, \omega)$ contains all information regarding other properties, such as the gradual loss in intensity of the signal (attenuation) and how its energy is spread out (spherical divergence) (Evrett, 2013; Park et al., 1998).

The Fourier transform of the recorded wavefield $(\tilde{u}(x, \omega))$ can equivalently be expressed in standard form as:

$$\tilde{u}(x, \omega) = A(x, \omega) e^{-i\Phi(\omega)x} \tag{6.2.10}$$

utilizing that:

$$P(x, \omega) = e^{-i\Phi(\omega)x} \tag{6.2.11}$$

The function $\Phi(\omega)$ has been identified as a type of a wave number spectrum:

$$\Phi(\omega) = \frac{\omega}{V_R(\omega)} \tag{6.2.12}$$

where $V_R(\omega)$ is the phase velocity at angular frequency ω (Park et al., 1998).

Considering each discrete trace separately, Eq. (6.2.5), can similarly be expressed as the product of amplitude $A_j(\omega)$ and phase $P_j(\omega)$ (Ryden et al., 2004):

$$\tilde{u}_j(\omega) = A_j(\omega)P_j(\omega) \qquad j = 1, 2, \ldots, n \tag{6.2.13}$$

The phase term in Eq. (6.2.13) ($P_j(\omega)$) is determined by the phase velocity of each frequency component according to:

$$P_j(\omega) = e^{-i\Phi(\omega)x_j} \tag{6.2.14}$$

$$\Phi(\omega)x_j = \frac{\omega x_j}{V_R(\omega)} = \frac{\omega(x_1 + (j-1)dx)}{V_R(\omega)} \qquad j = 1, 2, \ldots, n \tag{6.2.15}$$

where x_1 is the source offset and dx is the receiver spacing.

As all information regarding the phase velocity of each frequency component is contained in $P_j(\omega)$, the amplitude of each trace (in the frequency domain) can be normalized without loss of vital information according to (Ryden et al., 2004):

$$\tilde{u}_{j,norm}(\omega) = \frac{\tilde{u}_j(\omega)}{|\tilde{u}_j(\omega)|} = P_j(\omega) \tag{6.2.16}$$

$\tilde{u}_{j,norm}(\omega)$ is the normalized representation (in the frequency domain) of the j-th trace of the recorded wavefield.

6.2.2   Dispersion imaging

The fundamental idea the phase-shift method is based on, is shown in Figure 6.8. Figure 6.8(a) shows an array of normalized sinusoid curves. The curves can be thought of as multiple normalized traces from an n-channel impulsive shot gather after a Fourier transform has been applied to the recorded wavefield. The frequency of the sinusoid curves is assumed to be constant at 20 Hz and they are assumed to propagate at a phase velocity of 140 m/s (MASW, n.d.c).
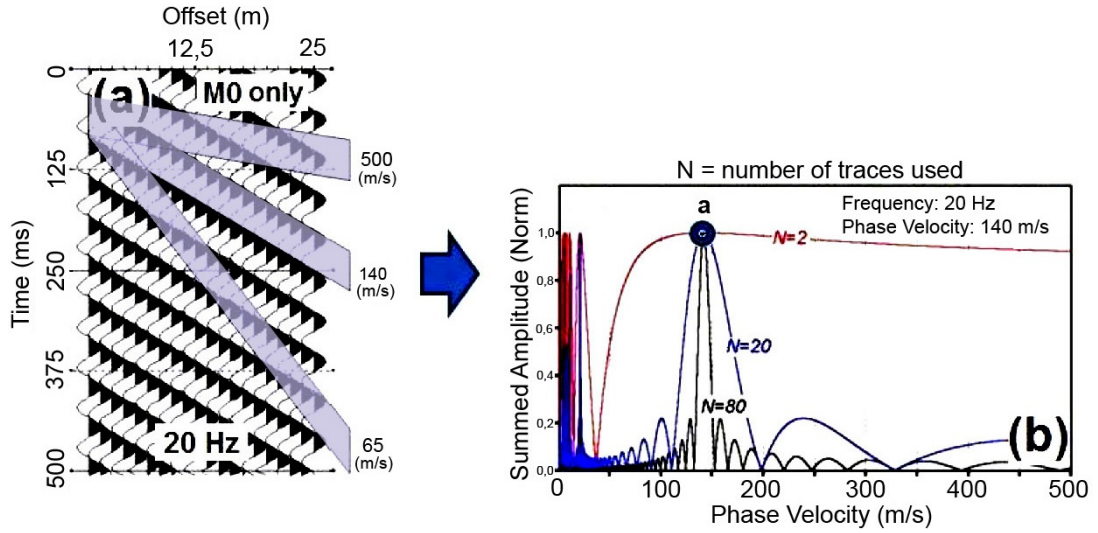
Figure 6.8: The basic principle behind the phase-shift method. (a) Normalized sinusoid curves with frequency of 20 Hz and phase velocity of 140 m/s. (b) Normalized summed amplitude as a function of frequency for different number of traces (MASW, n.d.c).

The sinusoid curves in Figure 6.8(a) have the same phase along the slope corresponding to the actual phase velocity (140 m/s) as indicated in the figure. However, the phase of the curves varies along the slopes corresponding to other phase velocities. If the curves are added along the slope of 140 m/s, their sum will be another sinusoid curve of finite length with amplitude $A_s = n$ (normalized summed amplitude $A_{s,norm} = 1$), as the amplitude of individual normalized curves is 1 and the number of curves is n. If the curves are added together along any other slope, i.e. corresponding to phase velocity of 65 m/s or 500 m/s, the amplitude of the resulting curve will be less than n (normalized summed amplitude less than 1). This is shown in Figure 6.8(b). The point marked with an **a** corresponds to the summed amplitude along the slope of 140 m/s (MASW, n.d.c; Ryden et al., 2004). The process of summing or stacking amplitudes in the offset domain along slanted paths is generally known as slant-stacking (Yilmaz, 2008).

Also indicated in Figure 6.8(b) is that the resolution of the dispersion image, implied by the sharpness of the peaks, generally increases with increasing number of geophones used for recording (MASW, n.d.c; Ryden et al., 2004).

Based on the previous description, the slant-stack function $\tilde{v}(\omega, V_{R,T})$ is defined according to the following integral transformation (Park et al., 1998):

$$\tilde{v}(\omega, V_{R,T}) = \int_{x_1}^{x_n} e^{i\phi x} \frac{\tilde{u}(x,\omega)}{|\tilde{u}(x,\omega)|} dx = \int_{x_1}^{x_n} e^{i\phi x} \tilde{u}_{norm}(x,\omega) dx \qquad (6.2.17)$$

where ϕ is the angular wavenumber corresponding to testing phase velocity $V_{R,T}$, given by:

$$\phi = \frac{\omega}{V_{R,T}} \qquad (6.2.18)$$

$\tilde{v}(\omega, V_{R,T})$ is the slant-stack amplitude for each combination of angular frequency (ω) and testing phase velocity ($V_{R,T}$). The lengths x_1 and $x_n = x_1 + L$ are the minimum and maximum source-receiver offsets, respectively.

The integral transformation in Eq. (6.2.17) includes summing over offsets of wavefields of a given frequency, after applying an offset-dependent phase shift determined for a given testing phase velocity ($V_{R,T}$). The normalization in Eq. (6.2.17) is applied in order to assure equal weighting of traces from different offsets and gain control of effects of spherical divergence and attenuation (Park et al., 1998).

By inserting Eq. (6.2.11) into Eq. (6.2.17), the following equation is obtained:

$$\tilde{v}(\omega, V_{R,T}) = \int_{x_1}^{x_n} e^{-i(\Phi(\omega)-\phi)x} \frac{A(x,\omega)}{|A(x,\omega)|} dx \qquad (6.2.19)$$

For a given ω, the maxima of $\tilde{v}(\omega, V_{R,T})$ will occur where:

$$\phi = \Phi(\omega) \qquad (6.2.20)$$

as the amplitude spectrum ($A(x,\omega)$) is real valued and positive (Park et al., 1998).

Utilising Eqs. (6.2.12) and (6.2.18), Eq. (6.2.20) can be written as:

$$\frac{\omega}{V_{R,T}} = \frac{\omega}{V_R(\omega)} \Leftrightarrow V_{R,T} = V_R(\omega) \qquad (6.2.21)$$

Thus, in order to determine the dispersion characteristics of $u(x,t)$, the values of $\tilde{v}(\omega, V_{R,T})$ are examined. When the testing phase velocity ($V_{R,T}$) is equal to the actual phase velocity corresponding to a given frequency ($V_R(\omega)$), a maxima will be observed in $\tilde{v}(\omega, V_{R,T})$. Joining together the peak values of $\tilde{v}(\omega, V_{R,T})$, for different values of ω, will generate the modal dispersion characteristics. If higher modes get substantial amount of energy, there will be two (or multiple) peak values for a given frequency, displaying the multi-modal characteristics of the recorded surface waves (Park et al., 1998; Ryden et al., 2004).

In practice the procedure is to vary $V_{R,T}$, for a given frequency ω, numerically evaluate the integral in Eq. (6.2.17) and study the maxima of $\tilde{v}(\omega, V_{R,T})$. The phase velocity is changed in small increments within a previously specified interval:

$$V_{R,T,min} \leq V_{R,T} \leq V_{R,T,max} \qquad (6.2.22)$$

By utilizing Eq. (6.2.16), Eq. (6.2.17) can be written in discrete form as:

$$\tilde{v}_s(\omega, V_{R,T}) = \sum_{j=1}^{n} e^{-i\phi x_j} \tilde{u}_{j,norm}(\omega) = \sum_{j=1}^{n} e^{-i\phi x_j} P_j(\omega) \qquad (6.2.23)$$

where:

$$\phi x_j = \frac{\omega x_j}{V_{R,T}} = \frac{\omega(x_1 + (j-1)dx)}{V_{R,T}} \qquad j = 1, 2, \ldots, n \qquad (6.2.24)$$

The values of $\tilde{v}_s(\omega, V_{R,T})$, obtained by Eqs. (6.2.23) and (6.2.24), are complex numbers whose absolute value $A_s(\omega, V_{R,T}) = |\tilde{v}_s(\omega, V_{R,T})|$ is the same as the summed (slant-stacked) amplitude for testing phase velocity $V_{R,T}$ and frequency ω. At each distinct frequency, the value of $V_{R,T}$ that gives the maximum value of A_s is the value being sought. If higher modes get enough energy, two (or more) distinct maxima will emerge for a given frequency, i.e. corresponding to different values of $V_{R,T}$ (Park et al., 1998; Ryden et al., 2004). As the maximum obtainable value of A_s depends on n, the number of geophones used for data acquisition, A_s should be normalized over the whole range of $V_{R,T}$ and ω according to Eq. (6.2.25) so that the peak value is 1 in all cases.

$$A_{s,norm}(\omega, V_{R,T}) = \frac{A_s(\omega, V_{R,T})}{\max\limits_{\omega, V_{R,T}} \{A_s(\omega, V_{R,T})\}} \qquad (6.2.25)$$

The results obtained by Eq. (6.2.23) for a given frequency ω and different values of $V_{R,T}$ can be represented by a plot of $V_{R,T}$ versus $A_{s,norm}$ as seen in Figure 6.8(b). In Figure 6.8(b), the value of $V_{R,T}$ being sought is the one corresponding to the maximum amplitude (denoted by an **a** in Figure 6.8) (MASW, n.d.c; Ryden et al., 2004).

However, the results are usually presented by a two-dimensional dispersion image obtained by plotting the values of $A_{s,norm}$ in the frequency – phase velocity - normalized summed amplitude domain, e.g. as a contour plot where different amplitudes are shown using a color scale. The high-amplitude bands observed will display the dispersion characteristics of the recorded surface waves (see Figure 6.9). Alternatively, the dispersion image can be presented in three dimensions where the dispersion characteristics are both indicated by the height of the peaks observed and a color scale (see Figure 6.10).
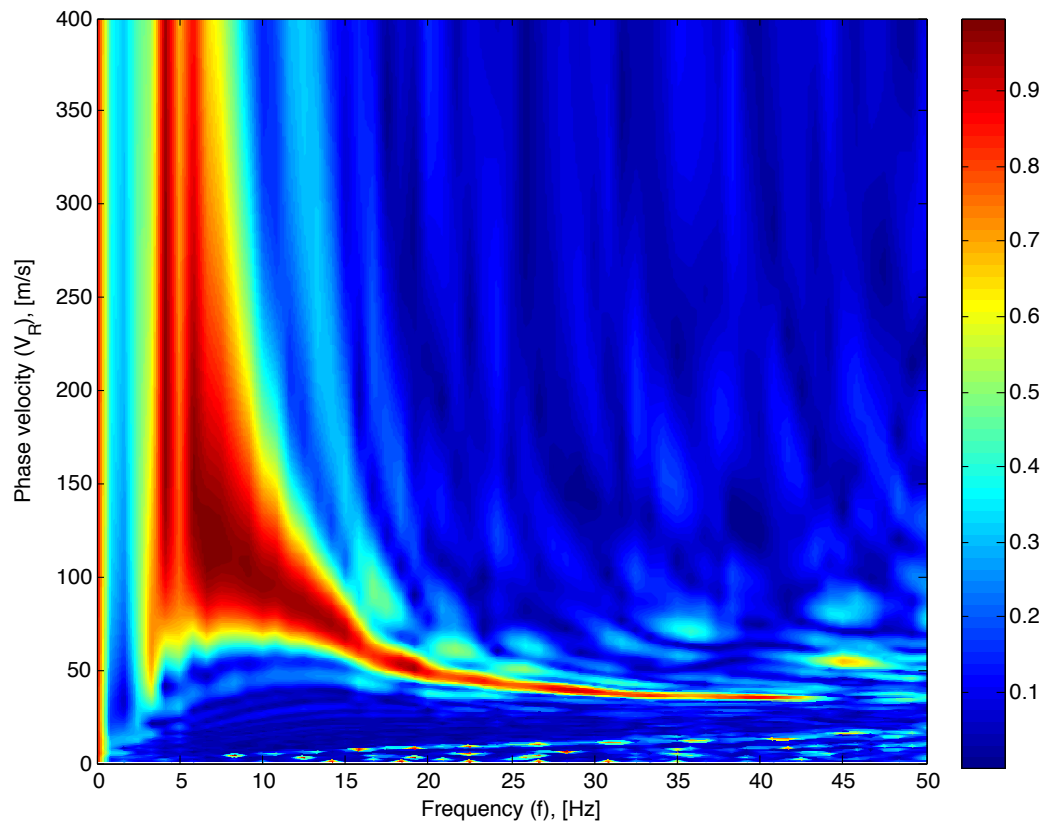
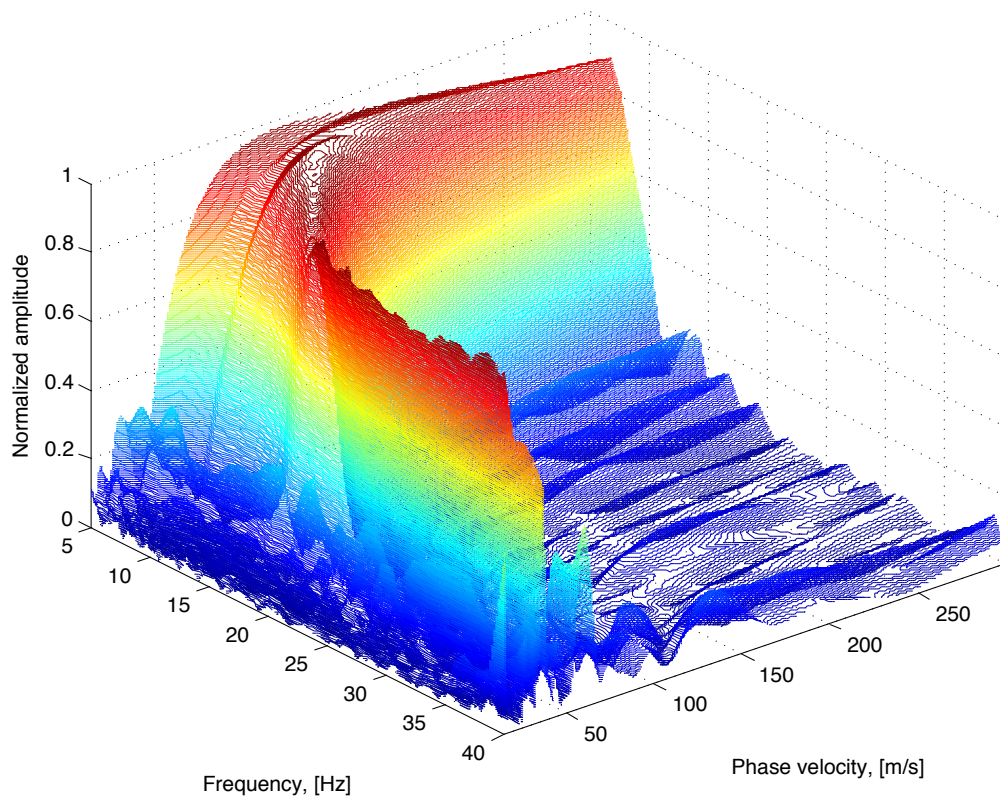Figure 6.9: Two dimensional dispersion image obtained by the phase-shift method.

Figure 6.10: Three dimensional dispersion image obtained by the phase-shift method.

6.2.3 Extraction of dispersion curves

Based on the energy content of the recorded surface wave wavefield, one or multiple dispersion curves can be extracted from the phase velocity spectra. The fundamental mode dispersion characteristics are usually of the most interest as the most commonly used inversion methods utilize only the fundamental mode dispersion curve (MASW, n.d.d) (see Chapter 7). However, due to reported advantages of multi-modal inversion (see Section 7.4), extraction of multi-modal dispersion curves (Xia, Miller & Park, 2000b) is worth noticing.

It is essential to avoid mode-number misidentification and mode-mix when dispersion curves are extracted from a phase velocity spectra. Mode-number misidentification is said to have occurred if modes are incorrectly identified, i.e. a higher mode is incorrectly taken as the fundamental mode. Mode-mix means that a certain extracted dispersion curve, that is thought to represent a certain mode, indeed encompasses more than one mode. Both mode-number misidentification and mode-mix can lead to substantial errors in inverted shear wave velocity profiles (MASW, n.d.d; Ryden & Park, 2006).

The procedure presented in this report is based on the assumption that the fundamental mode is the dominating mode of the recorded wavefield. Thus, if higher mode domination occurs, it will lead to erroneous results due to mode-number misidentification. Moreover, the procedure is only capable of extracting the fundamental mode dispersion curve. Improving the procedure and subsequently developing an algorithm capable of detecting and separating dispersion curves corresponding to multiple modes of propagation remains future work.

The phase velocity spectrum is reduced before the fundamental mode dispersion curve is extracted. That is, the values corresponding to the lowest phase velocities (V_R) and lowest frequencies (f) are removed in an attempt to minimize the risk of other seismic waves interrupting the resulting dispersion curve. The cut-off values of V_R and f must be manually adjusted to each site investigated.

The global maximum of the phase velocity spectrum (the maximum absolute summed amplitude, $A_{s,peak}$) is determined along with the corresponding frequency (f_{peak}) and phase velocity ($V_{R,peak}$). The phase velocity spectra is then divided into two parts based on frequency; values corresponding to $f > f_{peak}$ and values where $f < f_{peak}$.

For the part of the phase velocity spectra where $f > f_{peak}$, the maxima of A_s must all correspond to phase velocities lower than $V_{R,peak}$. Thus, for that part, only values of A_s where $V_R < V_{R,peak}$ are scanned in search of the maxima. This both prevents mode-mix at high frequencies and increases the speed of calculations.

Similarly, for the part where $f < f_{peak}$, the maxima must all correspond to phase velocity $V_R > V_{R,peak}$. Here, slight complications arise due to the rapid change of fundamental mode phase velocity with frequency. As the frequency axis is discrete with a frequency in-

crement limited by f_s/N (as indicated by Eqs. (6.2.3) and (6.2.8)), only a limited number of the peak values observed in the dispersion image can be extracted. Improved results can be obtained if the search is based on phase velocity instead of frequency. That is, for each value of $V_R > V_{R,peak}$, the peak value of A_s is determined with the constriction that only one value, the highest one, may correspond to each value of $f < f_{peak}$. Difficulties also arise when determining where the low frequency dispersion curve is reliable. Further work is required to study is accuracy of the dispersion curve at the lowest frequencies.

The dispersion curve is by convention presented as phase velocity vs. wavelength. The frequency-axis of the dispersion image is transformed using the relation between wavelength, frequency and Rayleigh wave phase velocity given by Eq. (2.2.1).

Figure 6.11 shows a three dimensional dispersion image where maxima corresponding to each frequency component in the range of 10 Hz to 39 Hz have been extracted. The extracted peak values corresponding to frequencies 12.5 Hz and 33.3 Hz are specially indicated by enlarged green markers. The dispersion curve obtained from the dispersion image, presented as phase velocity vs. wavelength, is shown in Figure 6.12. Points corresponding to the marked maxima in Figure 6.11 are indicated by green markers in Figure 6.12.
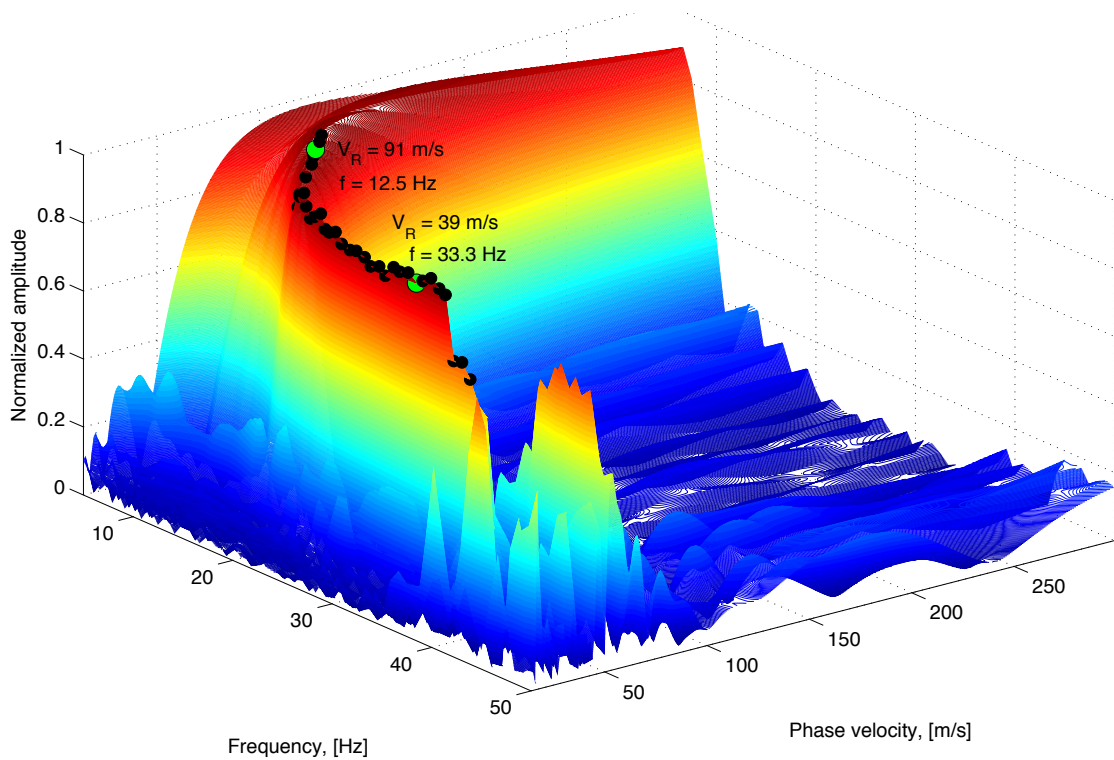

Figure 6.11: Fundamental mode dispersion characteristics extracted from a three dimensional dispersion image obtained by the phase-shift method. Maxima corresponding to frequency components in the range of 10 Hz to 39 Hz are indicated by black markers. The maxima corresponding to frequencies 12.5 Hz and 33.3 Hz are indicated by enlarged green markers.
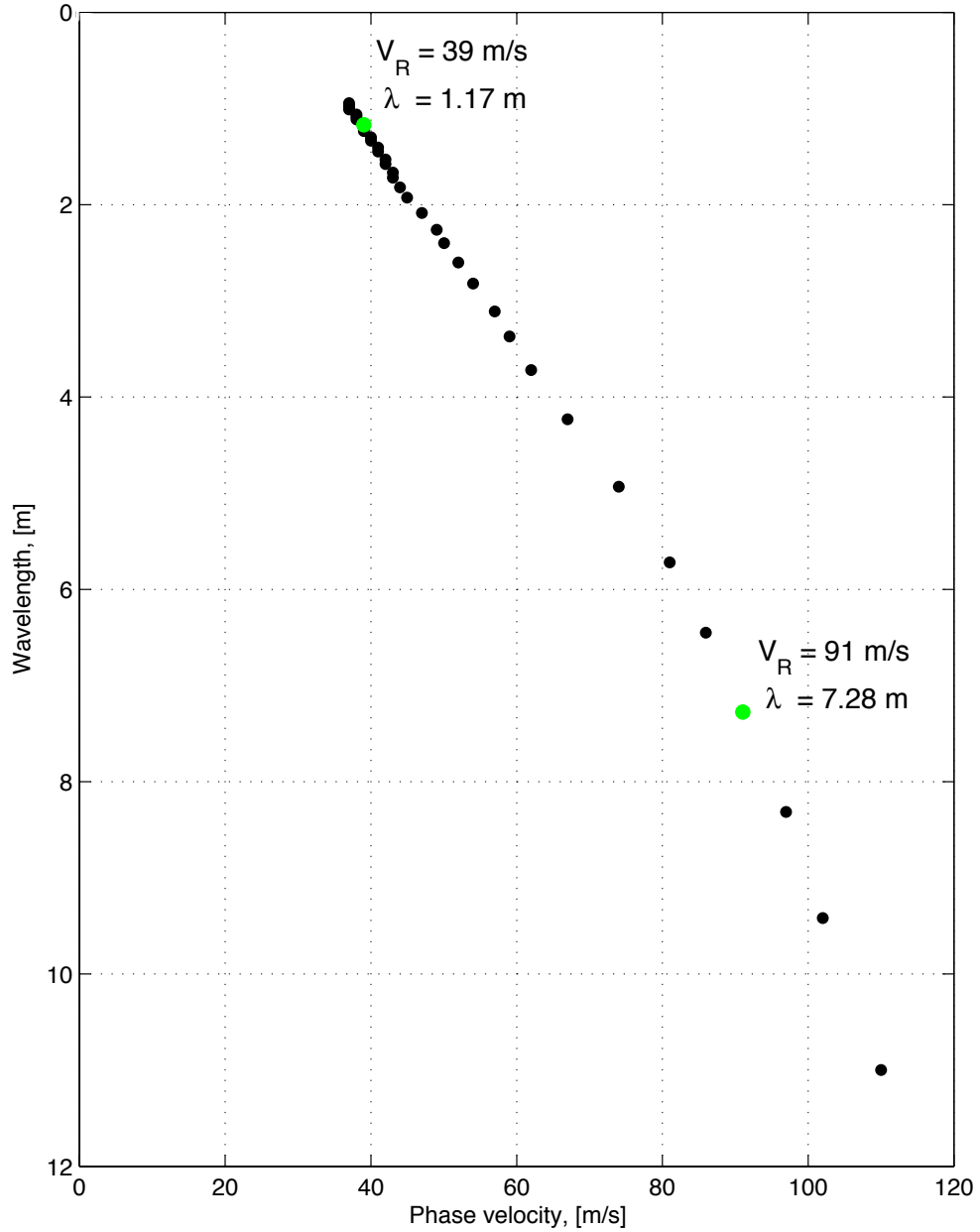
Figure 6.12: Fundamental mode dispersion curve obtained from the dispersion image shown in Figure 6.11. Points corresponding to the marked maxima in Figure 6.11 are indicated by green markers.

Chapter 7

Inversion analysis

The third and final step of both the MASW method and the SASW method is to derive a shear wave velocity profile, generally by inversion of the fundamental mode Rayleigh wave dispersion curve (MASW, n.d.d) as indicated in Figure 4.1. Calculations are based on wave propagation theory, assuming a layered earth model (Xia et al., 1999).

In general, an inverse problem consists of using results of measurements to estimate the values of the parameters that characterize the system under study. A forward problem addresses the reverse, i.e. predicting the results of measurements for a given set of model parameters (Tarantola, 2005). More specifically, the inverse problem confronted in both the MASW method and the SASW method consists of estimating the set of parameters that describe the soil deposit, based on an experimental dispersion curve.

Inversion problems based on wave propagation theory cannot be solved in a direct way due to their non-linearity. Thus, iterative methods where a theoretical dispersion curve is determined for a given layer model and compared to the previously obtained experimental dispersion curve must be used (Ryden et al., 2006).

This chapter provides a general overview of the inversion analysis involved in both the MASW method and the SASW method. Further study on different inversion methods, utilization of chosen procedures and software development remains future work.

7.1   Layered earth model and model parameters

The dispersion characteristics of a layered earth model depend on several groups of earth properties, such as number and thickness of soil layers and the elastic properties of each layer. Figure 7.1 shows a generalized example of a layered earth model. The elastic properties of individual layers are generally represented by at set of more easily measurable physical properties, i.e. compressional wave velocity (V_P), shear wave velocity (V_S) and mass density (ρ) (MASW, n.d.d; Xia et al., 1999). The properties within each layer are taken as constant and the last layer is assumed to be a half-space (Xia et al., 1999).

For a layered earth model, the shear wave velocity profile has a dominant effect on the fundamental mode dispersion curve, followed by layer thickness (Xia et al., 1999). As the

effect of change in compressional wave velocity and density is insignificant (Tokimatsu, Member, Tamura & Kojima, 1991), these parameters are often assumed known.
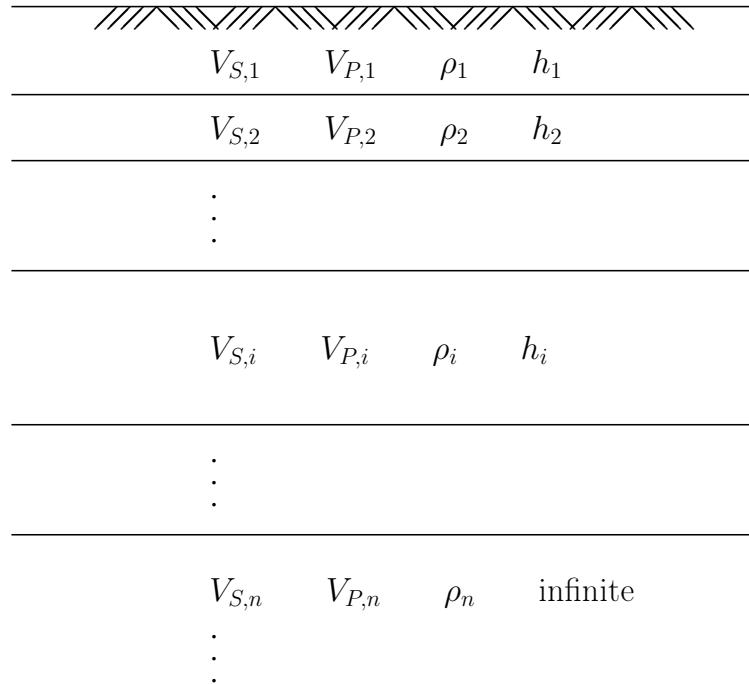

Figure 7.1: Layered earth model for inversion analysis. The parameters of the model are body wave velocities, V_S and V_P, mass density, ρ, and thickness of layers, h. The last layer is assumed to be a half-space.

By assuming a layered model with no lateral variation, the resulting shear wave velocity profile becomes one-dimensional. The profile obtained gives therefore the shear wave velocity structure that is the most representative of the subsurface materials below the receiver spread, approximating them as a layered even though some lateral variation does exist. It is customary to assign the shear wave velocity profile obtained to the center of the receiver spread if a unique surface coordinate is required (MASW, n.d.d).

7.2   General inversion algorithms

A mathematical model for layered elastic material is used to determine a theoretical dispersion curve based on a given set of input parameters. Different sets of parameters are inserted into the model in an iterative way in search of the theoretical dispersion curve that is the most consistent with the observed dispersion characteristics. Thus, the problem of obtaining an acceptable shear wave velocity profile can be identified as a multi-parameter optimization problem where the objective is to minimize the difference between the experimental and theoretical dispersion curves. The root-mean-square error between the two data sets is commonly used as an indicator of the difference between the theoretical and the experimental dispersion curves (MASW, n.d.d; Orozco, 2003; Xia et al., 1999).

Various algorithms have been developed and used for inversion of experimental surface wave data. Possible inversion procedures can be divided into two categories; *local search* and *global search procedures*. The division is based on how model parameters are updated between iterations during search for the most probable set of parameters (Orozco, 2003).

A schematic overview of a typical local inversion algorithm is shown in Figure 7.2 (Orozco, 2003).
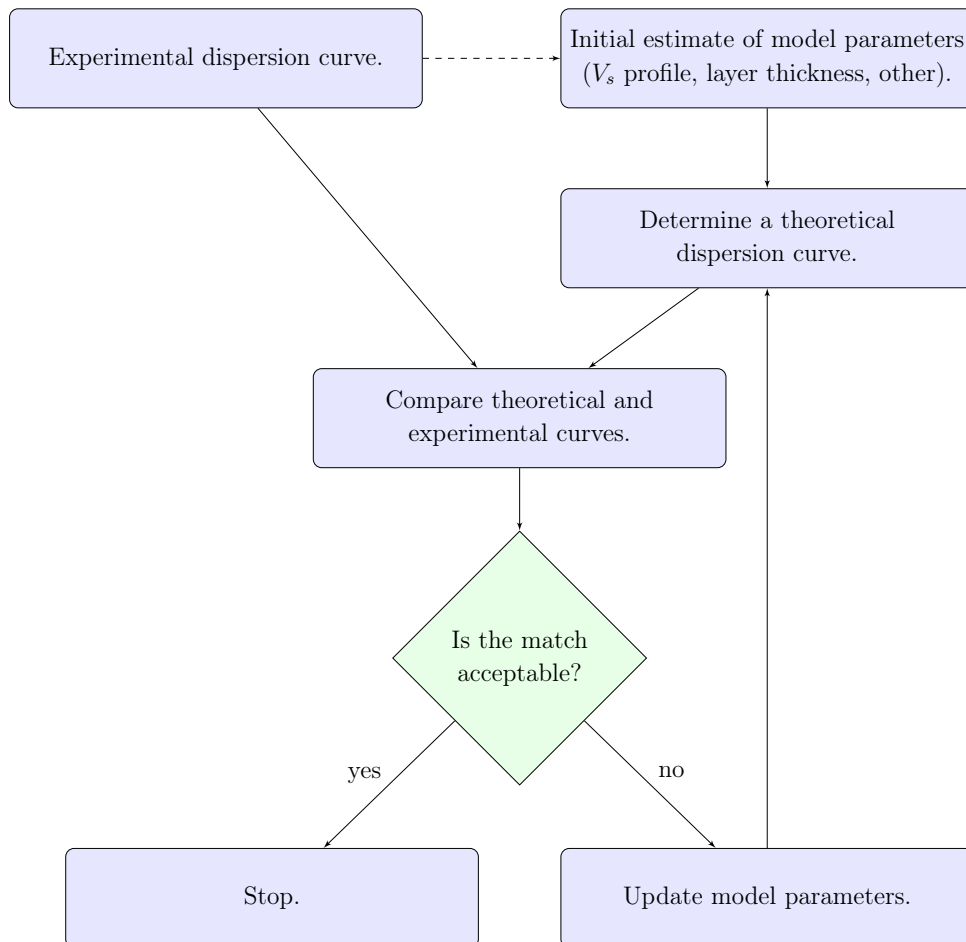

Figure 7.2: Overview of a typical local inversion algorithm.

The first step of a typical local inversion algorithm is to make an initial estimate of the required model parameters. A reasonable initial guess is essential, as convergence of the algorithm can only be guarantied if the initial set of model parameters is sufficiently close to the final solution. Based on the initial estimate, a theoretical dispersion curve is determined. If the difference between the experimental curve and the theoretical curve is acceptable, the problem is considered solved. Otherwise, the set of model parameters is updated. A new theoretical dispersion curve is determined and compared to the experimental dispersion characteristics. The iterations continue until a reasonable match, in the vicinity of the initial estimate, is found or until the maximum number of iterations is obtained. If the method does not converge, the initial set of model parameters must be changed (Orozco, 2003; Xia et al. 1999).

In global procedures, it is attempted to search the entire solution space for the global minimum of the difference between a theoretical dispersion curve and the experimental data (Orozco, 2003). A conventional approach is to randomly generate parametric sets within a previously specified range. Such methods, that both involve iteration and a random generator, are referred to as Monte Carlo methods (Socco & Boiero, 2008). The set of parameters that result in the theoretical dispersion curve that best fits the experimental data is taken as the result of the survey.

Both local and global search methods have certain advantages and disadvantages. The main advantage of local methods is considerably better computational speed as compared to global methods. However, solutions obtained by local methods are generally strongly biased by the initial guess. The risk of finding a local minimum instead of the global minimum is thus substantial when local search methods are applied (MASW, n.d.d; Socco & Boiero, 2008).

7.3 Theoretical dispersion curves

Theoretical dispersion curves are generally determined by matrix methods based on wave propagation theory. Thomson (1950) and Haskell (1953) formulated and presented the forward problem of surface wave propagation and dispersion in a layered media. The Thompson-Haskell method of determining surface wave dispersion curves is based on the use of transfer matrices in the frequency-wavenumber domain (Haskell, 1953) and thus also commonly referred to as the *transfer matrix method*. Based on the Thomson-Haskell method, various methods have been developed to study surface wave propagation in layered media. Commonly used methods include the approaches introduced by Schwab and Knopoff (1970) and Kausel and Roësset (1981).

The *Schwab-Knopoff method* is, as well as the Thomson-Haskell formulation, based on transfer matrices. However, the main advantage of the Schwab-Knopoff approach, as compared to the Thomson-Haskell method, is increased speed of calculations and reduction of overflow and loss-of-precision problems, thus resulting in increased accuracy (Schwab & Knopoff, 1970).

Kausel and Roësset (1981) presented an alternate formulation of the Haskel-Thompson method using stiffness matrices, similar to those used in conventional structural analysis (the finite element method). An element stiffness matrix is obtained for each layer, formulated in the frequency domain. The element stiffness matrix of a distinct layer relates the stresses at the interfaces of the layer to the corresponding displacements. For a multilayered model, the element stiffness matrices are assembled utilizing common degrees of freedom (layer interfaces) to form a global stiffness matrix. The global stiffness matrix is then used, along with the prescribed (global) external stresses at the layer interfaces, to solve for the displacements with techniques analogous to those used in the finite element method.

7.4   Multi-modal and dispersion image inversion

In attempt to increase the accuracy of the shear wave velocity profile obtained by a MASW survey, alternative inversion methods have been developed where the inversion is not only based on the fundamental mode dispersion curve. These include *multi-modal inversion methods* and *dispersion image inversion methods* (Ryden & Park, 2006, Xia et al., 2000b).

In multi-modal inversion procedures, higher mode dispersion curves are used along with the fundamental mode curve. Reported advantages include increased investigation depth and a more stable inversion process, ultimately resulting in an increased resolution of the shear wave velocity profile (Xia et al., 2000). Others claim that added complexity does only make the problem more difficult to handle, without improving the outcome (MASW, n.d.d).

Dispersion image inversion involves inverting the entire dispersion image without extracting any modal dispersion curves. By inverting the whole phase velocity spectra, it is possible to avoid the risk of mode-misidentification and mode-mix. The main disadvantage of this approach is much longer computational time than required in traditional fundamental mode based inversion procedures (Ryden & Park, 2006).

Chapter 8

Conclusions and future work

Multichannel Analysis of Surface Waves (MASW) is a seismic exploration method to estimate the shear wave velocity profile of near-surface materials. This method was first introduced in the late 1990s and is now applied for the first time in Iceland.

The MASW method is generally divided into three main steps; data acquisition, dispersion analysis and inversion analysis. This report provides a comprehensive description of the data acquisition and dispersion analysis steps. Two different dispersion analysis methods are described in detail, a swept-frequency approach and the phase-shift method.

The main advantages of the MASW method over the SASW method include a more efficient data acquisition routine in the field, faster and less labor consuming data processing procedures and improved identification and elimination of noise from recorded data. Moreover, by using the MASW method, it is possible to observe the multi-modal dispersion characteristics of recorded surface waves and the generation of two (or three) dimensional dispersion images becomes possible and economically feasible.

During the fall of 2013 and the summer of 2014 MASW field measurements were carried out at a few sites in South Iceland. The data obtained was used to write and test a data processing program, developed using the computational software Matlab. Selected results are presented in Appendix A. Results of preliminary testing are promising and the dispersion curves obtained with the phase-shift method and the swept-frequency approach are comparable.

The dispersion analysis program still requires comprehensive testing and validation, using surface wave data from several different sites, where comparison with results obtained by other measurement techniques, such as the SPT and CPT methods, is possible. Performing MASW field measurements at sites with different soil characteristics also helps evaluating the versatility of the method and the proposed algorithm. Moreover, to study the effect of the data acquisition parameters, data should be gathered with several source-receiver configurations using different seismic sources. Emphasis should be on the low frequency (long wavelength) part of the obtained dispersion curve, as the interval where the results are reliable has to be determined.

The phase-shift method algorithm is believed to have more potential for further improvement. The procedure presented in this report is based on the assumption that the fundamental mode is the dominating mode of the recorded wavefield. Thus, if higher mode domination occurs, it will lead to erroneous results due to mode-number misidentification. Moreover, the procedure is only capable of extracting the fundamental mode dispersion curve. Improving the procedure and subsequently developing an algorithm capable of detecting and separating dispersion curves corresponding to multiple modes of propagation is therefore of interest.

A general overview of the inversion analysis involved in the MASW method is provided in this report. Future steps of the project include further study on different inversion methods, utilization of chosen procedures and software development for inversion analysis with emphasis on automation of the inversion process and error estimations both at the dispersion analysis and the inversion analysis level.

References

Aki, K. & Richards, P. G. (2002). *Quantitative Seismology.* (Second edition). Sausalito, CA: University Science Books.

Bessason, B. & Erlingsson, S. (2011). Shear wave velocity in surface sediments. *Jökull 61*, 51-64.

Bradie, B. (2006). *A Friendly Introduction to Numerical Analysis.* Upper Saddle River, NJ: Pearson Education, Inc.

Bolt, B. B. (1976). *Nuclear Explosions and Earthquakes: The Parted Veil.* San Francisco, CA: W.H. Freeman and Company.

Donohue, S., Dermot, F. & Donohue, L. A. (2013). Detection of soil compaction using seismic surface waves. *Soil and Tillage Research, 128*, 54-60.

Evrett, M. E. (2013). *Near-Surface Applied Geophysics.* Cambridge: Cambridge University Press.

Foti, S. (2000). *Multistation Methods for Geotechnical Characterization using Surface Waves.* (Doctoral dissertation, Politecnico di Torino, Turin, Italy). Retrieved from http://porto.polito.it/2497212/1/S_Foti_PhDdiss.pdf

Gedge, M. & Hill, M. (2012). Acoustofluidics 17: Theory and applications of surface acoustic wave devices for particle manipulation. *Lab Chip, 12*(17), 2998-3007.

Haskell, N. A. (1953). The dispersion of surface waves on multilayered media. *Bulletin of the Seismological Society of America, 43*, 17–34.

Kaldal, L. S. (2007). *Yfirborðsmælingar og ysjunarhætta.* (Master's thesis). University of Iceland, Reykjavík.

Kausel, E. & Roësset, J. M. (1981). Stiffness matrices for layered soils. *Bulletin of the Seismological Society of America, 71*(6), 1743-1761.

Kreyszig, E. (2011). *Advanced Engineering Mathematics.* (10th Edition, International Student Edition). Hoboken, NJ: John Wiley & Sons, Inc.

Lin, C.-P., Chang, C.-C. & Chang, T.-S. (2004), The Use of MASW Method in the Assessment of Soil Liquefaction Potential. *Soil Dynamics and Earthquake Engineering, 24,* 689-698.

Luna, R. & Jadi, H. (2000). Determination of Dynamic Soil Properties Using Geophysical Methods. *Preceedings of the First International Conference on the Application of Geophysical and NDT Methodologies to Transportation Facilities and Infrastructure, St. Louis, December 2000.*

MathWorks. (n.d.). Documentation Center. imregionalmax. Retrieved May 10, 2014 from http://www.mathworks.se/help/images/ref/imregionalmax.html

McMechan, G. & Yedlin, M. J. (1981). Analysis of dispersive waves by wave field transformation. *Geophysics, 46*(6), 869-874.

Multichannel Analyses of Surface Waves (MASW). (n.d.a). Data Acquisition. Retrieved May 10, 2014 from http://www.masw.com/DataAcquisition.html

Multichannel Analyses of Surface Waves (MASW). (n.d.b). Dispersion Imaging Scheme. Retrieved May 10, 2014 from http://www.masw.com/DCImagingScheme.html

Multichannel Analyses of Surface Waves (MASW). (n.d.c). Dispersion Imaging Scheme. Summary of Park et al., 1998a. Retrieved May 10, 2014 from http://www.masw.com/files/DispersionImaingScheme-1.pdf

Multichannel Analyses of Surface Waves (MASW). (n.d.d). Inversion Analysis of Surface Waves. Retrieved May 10, 2014 from http://www.masw.com/InversionAnalysis.html

Multichannel Analyses of Surface Waves (MASW). (n.d.e). What is dispersion? Retrieved May 10, 2014 from http://www.masw.com/Whatisdispersion.html

Orozco, M. C. (2003). *Inversion Method for Spectral Analysis of Surface Waves (SASW).* (Doctoral dissertation, Georgia Institute of Technology, Atlanta, GA). Retrieved from https://smartech.gatech.edu/bitstream/handle/1853/5124/OROZCO_MARIA _C_200405_phd.pdf

Park, C. B., Miller, R. D. & Xia, J. (1997). *Summary report on surface-wave project at Kansas Geological Survey (KGS).* [Open-file Report]. Lawrence, KS: Kansas Geological Survey.

Park, C. B., Miller, R. D. & Xia, J. (1998). Imaging dispersion curves of surface waves on multichannel record. *68th Annual International Meeting Society of Exploration Geophysicists, Expanded Abstracts*, 1377-1380.

Park, C. B., Miller, R. D. & Xia, J. (1999). Multichannel analysis of surface waves. *Geophysics, 64*(3), 800-808.

Park, C. B., Miller, R. D., Xia, J. & Ivanov, J. (2000). Multichannel seismic surface-wave methods for geotechnical applications. *Proceedings of the First International Conference on the Application of Geophysical Methodologies to Transportation Facilities and Infrastructure, St. Louis, December 11-15, 2000.*

Park, C. B., Miller, R. D. & Xia, J. (2001). Offset and resolution of dispersion curve in multichannel analysis of surface waves (MASW). *Proceedings of the Symposium on the Application of Geophysics to Engineering and Environmental Problems (SAGEEP 2001), Denver, Colorado*, SSM-4.

Park, C. B., Miller, R. D. & Miura, H. (2002). Optimum field parameters of an MASW survey. *Expanded Abstracts, SEG-J, Tokyo, May 22-23, 2002.*

Park, C. B., Miller, R. D., Xia, J. & Ivanov, J. (2007). Multichannel analysis of surface waves (MASW) - active and passive methods. *The Leading Edge, 26*(1), 60-64.

Park, C. B. & Shawver, J. B. (2009). Multi-source offset MASW survey. *Proceedings of the Symposium on the Application of Geophysics to Engineering and Environmental Problems (SAGEEP 2009), Fort Worth, Texas, March 29-April 2.*

Park, C. B. and Carnevale, M. (2010). Optimum MASW Survey - Revisit after a Decade of Use. In Fratta, D. O., Puppala, A. J. & Muhunthan, B (editors), *GeoFlorida 2010: Advences in Analysis, Modeling and Design* (pp. 1303-1312). doi: 10.1061/41095(365)130

Ryden, N., Park, C. B., Ulriksen, P. & Miller, R. D. (2004). Multimodal approach to seismic pavement testing. *Journal of Geotechnical and Geoenvironmental Engineering, 130*, 636-645.

Ryden, N. & Park, C. B. (2006) Fast Simulated Annealing Inversion of Surface Waves on Pavements using Phase Velocity Spectra. *Geophysics, 71*(4), R49-R58.

Schilling, R. J. & Harris, S. L. (2012). *Introduction to Digital Signal Processing using MATLAB.* (International Edition. 2nd edition). Cengage Learning.

Sigbjörnsson, R. *Continuum Mechanics. Lecture notes.* Reykjavík: University of Iceland.

Schwab, F. A. & Knopoff, L. (1970). Surface-wave dispersion computations. *Bulletin of the Seismological Society of America, 60*, 321-344.

Socco, L. V. & Boiero, D. (2008). Improved Monte Carlo inversion of surface wave data. *Geophysical Prospecting, 56*(3), 1365-2478.

Sólnes, J., Sigmundsson, F. & Bessason, B. (Editors). (2013). *Náttúruvá á Íslandi - Eldgos og Jarðskjálftar*. Reykjavík: Viðlagatrygging Íslands & Háskólaútgáfan.

Stocia, P. & Moses, R. (2005). *Spectral Analysis of Signals*. Upper Saddle River, NJ: Prentice Hall, Inc.

Tarantola, A. (2005). *Inverse problem theory and methods for model parameter estimation*. Philadelphia, PA: Society for Industrial and Applied Mathematics.

Thomson, W. T. (1950). Transmission of elastic waves through a stratified solid medium. *Journal of Applied Physics, 21*, 89–93.

Tokimatsu, K., Kuwayama, S., Tamura, S. & Miyadera, Y. (1991). Effects of Multiple Modes on Rayleigh Wave Dispersion Characteristics. *Soils and Foundations, 31*(2), 153-163.

Vinh, P. C. & Malischewsky, P. G. (2007). An approach for obtaining approximate formulas for the Rayleigh wave velocity. *Wave Motion, 44*, 549-562.

Xia, J., Miller, R. D. & Park, C. B. (1999). Estimation of near-surface shear-wave velocity by inversion of Rayleigh waves. *Geophysics, 64*(3), 691-700.

Xia, J., Miller, R. D., Park, C. B. & Ivanov, J. (2000). Construction of 2-D vertical shear-wave velocity field by the multichannel analysis of surface waves technique. *Proceeding of the Symposium of the Application of Geophysics to Engineering Environmental Problems (SAGEEP 2000) Arlington, VA., February 20-24*, 1197-1206.

Xia, J., Miller, R. D., Park, C. B. (2000b). Advantages of calculating shear-wave velocity from surface waves with higher modes. *Society of Exploration Geophysicists, Expanded Abstracts*, 1295-1298.

Xia, J., Miller, R. D., Park, C. B., Hunter, J. A., Harris, J. B. & Ivanov, J. (2002). Comparing shear-wave velocity profiles from multichannel analysis of surface wave with borehole measurements. *Soil Dynamics and Earthquake Engineering, 22*(3), 181-190.

Xia, J., Miller R. D., Park C. B. & Tian G. (2003). Inversion of high frequency surface waves with fundamental and higher modes. *Journal of Applied Geophysics, 52*, 45-57.

Yilmaz, Ö. (2008). *Seismic Data Analysis: Processing, Inversion, and Interpretation of Seismic Data*. [Electronic Edition]. Tulsa, OK: Society of Exploration Geophysicsts.

Young, H. D. & Freedman, R. A. (2008). *University Physics with Modern Physics*. (12th Edition). San Francisco, CA: Pearson Addison-Wesley.

Zeng, C., Xia, J., Miller, R. D., Tsoflias, G. P. & Wang, Z. (2012). Numerical investigation of MASW applications in presence of surface topography. *Journal of Applied Geophysics, 84,* 52-60.

Wair, B. R., DeJong, J. T. & Shantz, T. (2012). *Guidelines for Estimation of Shear Wave Velocity Profiles.* Berkeley, CA: Pacific Earthquake Research Center.

Appendix A

Example: Field test with impulsive source

A field test was carried out close to Arnarbæli in South Iceland the 18th of September 2013. Impulsive data was acquired at two test sites referred to as Profile 1 and Profile 2 (see Figures A.1 and A.2). The main purpose of the measurements was to test the new MASW data acquisition equipment/software and gather records necessary for the development of a data processing software to extract Rayleigh wave dispersion curves from multichannel surface wave records.

Figure A.1: Location of MASW test measurements.

Figure A.2: Location of MASW test measurements. Impulsive data was acquired at two sites, here referred to as Profile 1 and Profile 2.

A.1 Field measurements

Data was recorded both by using a 7 kg sledgehammer as impact source and by jumping. Twenty-four 4.5Hz geophones of type GS11D from Geospace Technologies were lined up at the surface of the test sites (see Figure A.3). The geophones were connected to a data acquisition card (type NI USB-6218 from National Instruments) and a computer equipped with the customized MASW data gathering software written in Labview.

Figure A.3: MASW measurement profile at a test site near Arnarbæli in South Iceland. Lineup of 24 geophones with equal spacing of 1.0 m connected to a seismic cable.

For recording, a sampling rate (dt) of 1 ms was used, corresponding to a measuring frequency (f_s) of 1000 Hz. The total recording time (T) was 1.2 seconds. The receiver spacing (dx) was 1.0 m, corresponding to a receiver spread length (L) of 23.0 m. Data was gathered with varying source offset (x_1), i.e. 3 m, 5 m, 10 m and 20 m. Furthermore, data was gathered from both ends of the receiver line. For demonstration purposes, only dispersion curves obtained from selected measurements are presented.

Figures A.4 and A.5 show the recorded surface wave data obtained by Profile 1 (left) and Profile 2 (right) with source offset of $x_1 = 10$ m. The records show ground roll being picked up by all receivers without much noticable contamination of noise.
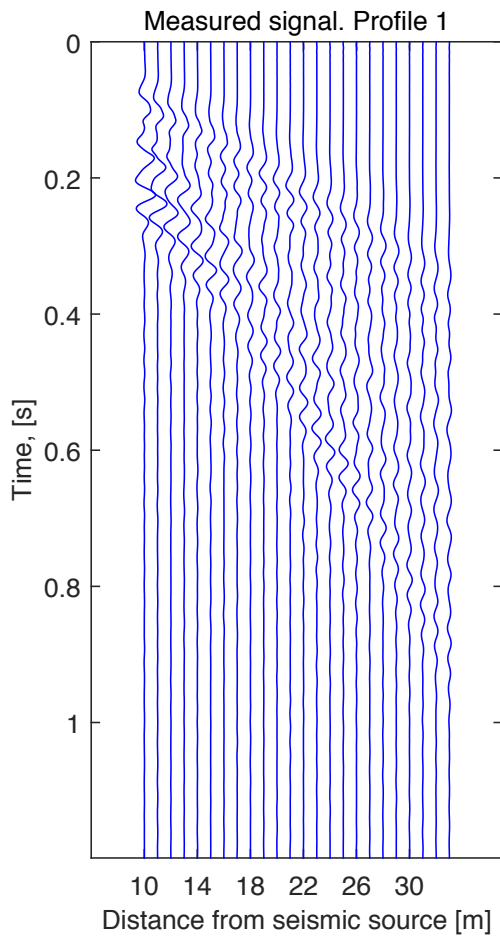
Figure A.4: Recorded surface wave data. 24-channel shot gather obtained at a test site near Arnarbæli. Profile 1.
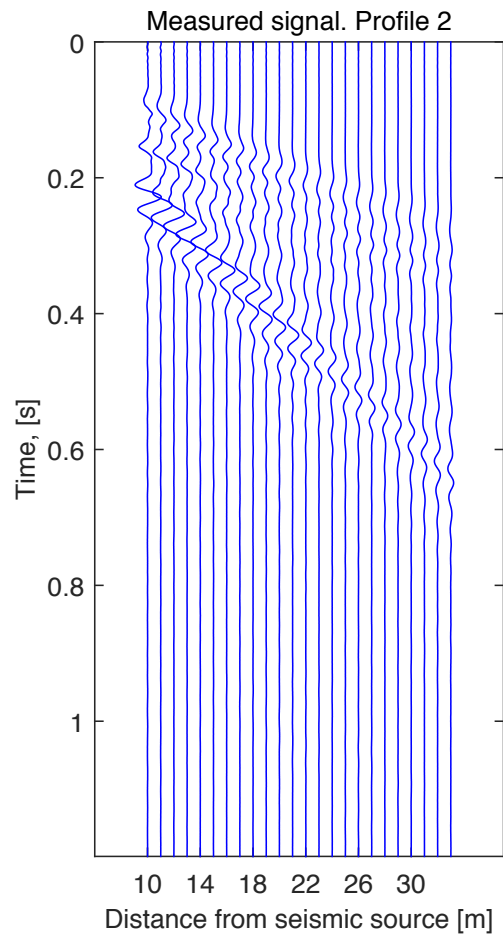
Figure A.5: Recorded surface wave data. 24-channel shot gather obtained at a test site near Arnarbæli. Profile 2.

A.2   Dispersion analysis

Both dispersion analysis methods presented in this report, the swept-frequency approach and the phase-shift method, were used to extract a fundamental mode dispersion curve from the data obtained at the Arnarbæli test site.

A.2.1   Application of the phase-shift method

A phase velocity spectra was obtained for the recorded surface wave data shown in Figures A.4 and A.5 using the phase-shift method. The resulting dispersion images are shown in Figures A.6 and A.7, represented in three dimensions. The high-amplitude bands observed in the three-dimensional dispersion images correspond to the dominating fundamental mode of the recorded surface waves. The smaller crests (at higher phase velocities than the fundamental mode bands) are due to the higher-mode content of the shot gather. The higher modes are visible in Figures A.6 and A.7 at frequencies of around 25 Hz and above. As the higher modes get substantially more energy, the fundamental mode peaks become less sharp (appear lower).

The marked points in Figures A.6 and A.7 correspond to the extracted fundamental mode dispersion curves. In Figure A.6 (Profile 1), an attempt is not made to extract peak values corresponding to higher frequencies than 25 Hz as the dispersion analysis software is not capable of separating higher modes from the fundamental mode if the fundamental mode is not the dominating mode. For Profile 2, where the sharpness of the fundamental mode peaks at higher frequencies is more, peak values corresponding to higher frequencies can be extracted.

The fundamental mode dispersion curve for each profile is presented as phase velocity vs. wavelength in Figures A.8 and A.9, respectively.
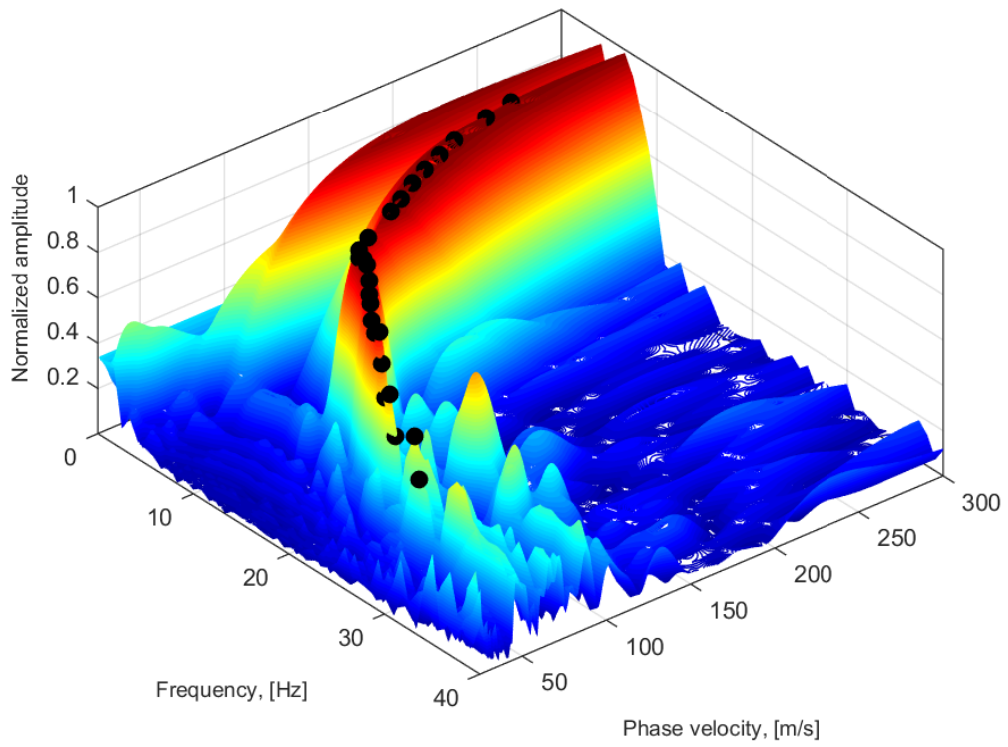
Figure A.6: Dispersion image obtained from the recorded surface wave data in Figure A.4 by using the phase-shift method. Profile 1.
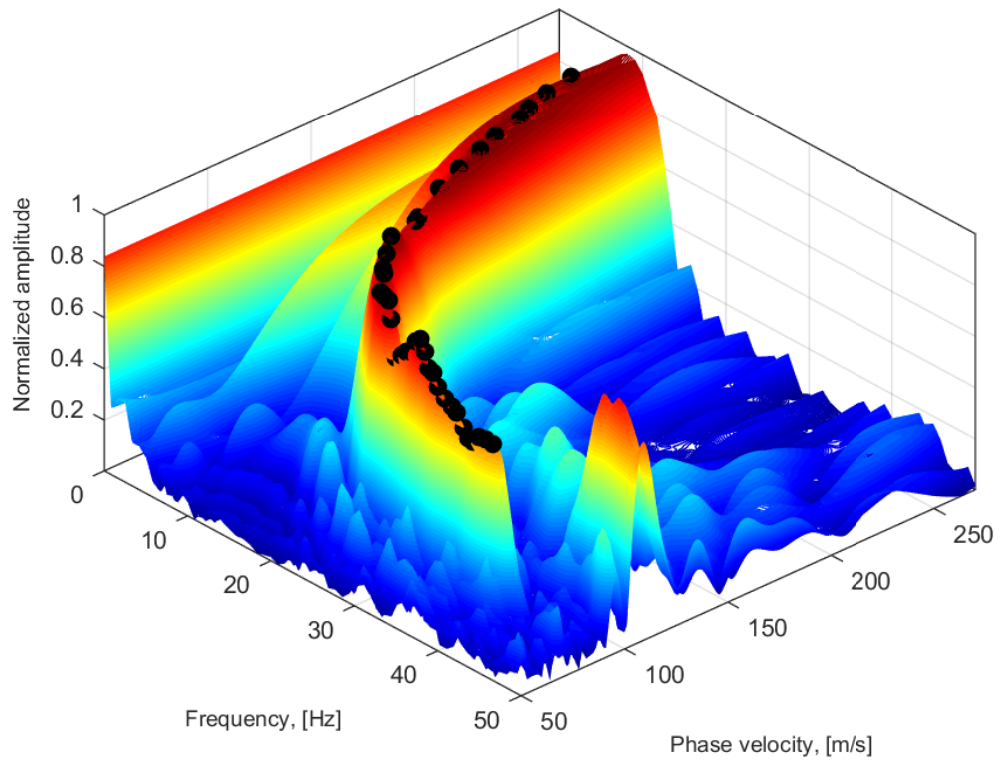

Figure A.7: Dispersion image obtained from the recorded surface wave data in Figure A.5 by using the phase-shift method. Profile 2.
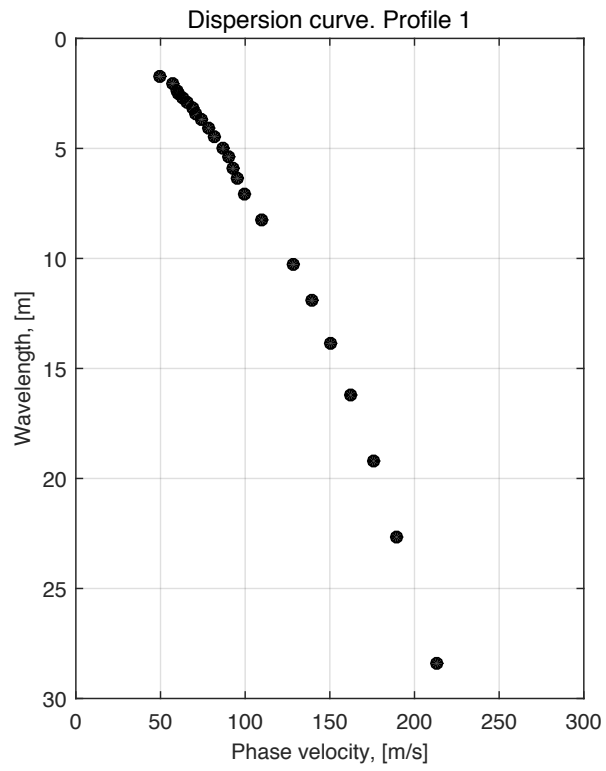
Figure A.8: Fundamental mode dispersion curve obtained from the dispersion image in Figure A.6. Profile 1.
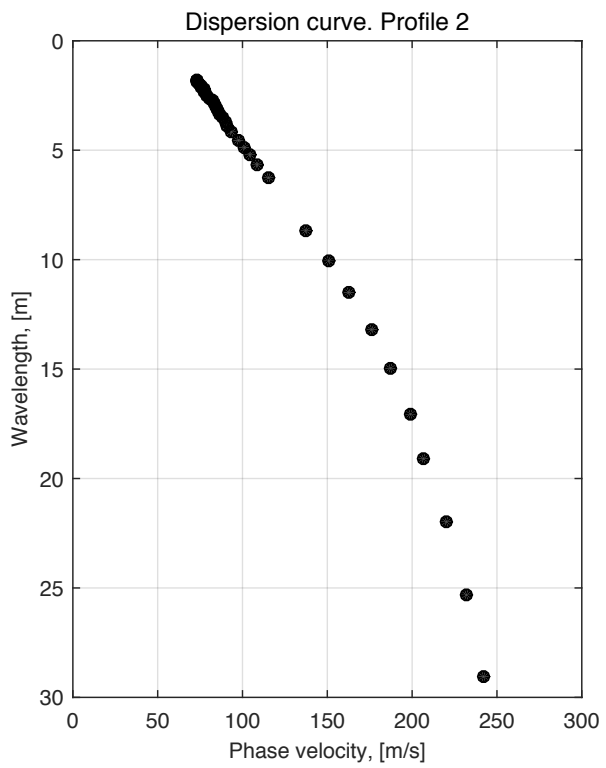

Figure A.9: Fundamental mode dispersion curve obtained from the dispersion image in Figure A.7. Profile 2.

A.2.2   Application of the swept-frequency approach

Swept-frequency records were obtained by convolution of the impulsive records (Figures A.4 and A.5) with a stretch function. The stretch function was chosen according to Eq. (6.1.5) with linearly changing frequency from $f_1 = 5$ Hz to $f_2 = 50$ Hz and of length $T = 10$ s. Figures A.10 and A.11 show the resulting 12-s long swept-frequency records.
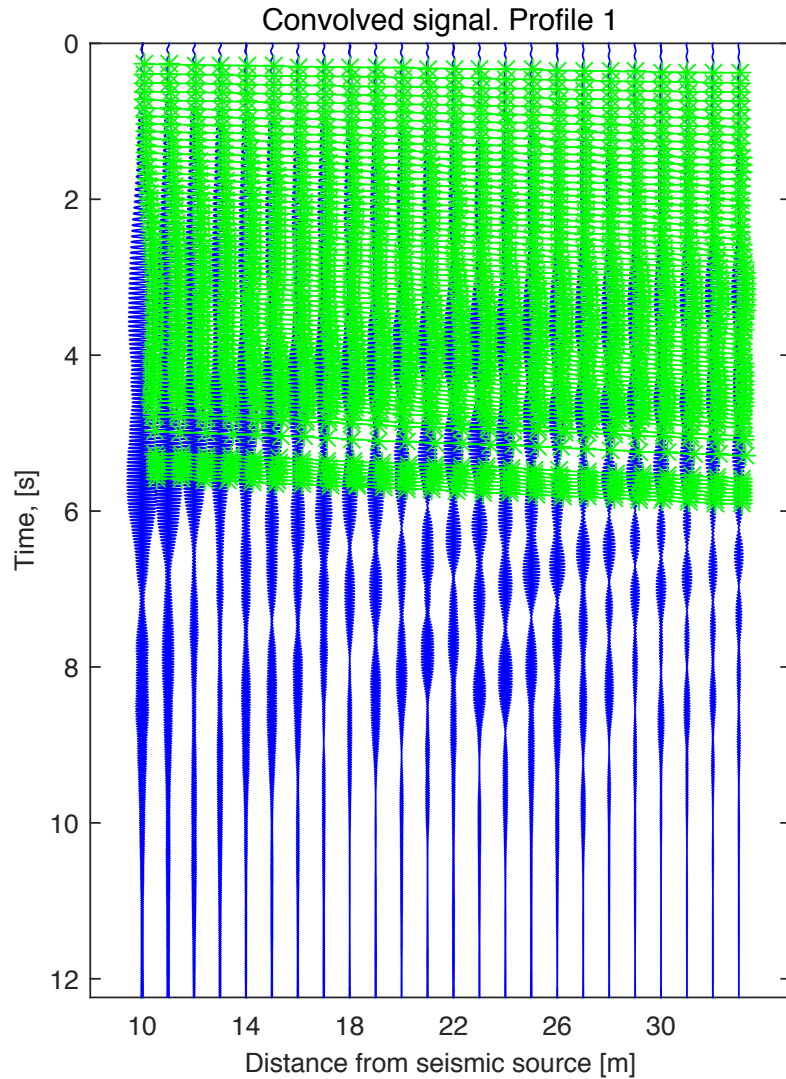
Figure A.10: A 24-channel swept-frequency record with linearly changing frequency from $f_1 = 5$ Hz to $f_2 = 50$ Hz obtained from the impulsive record in Figure A.4 by convolution. Profile 1.
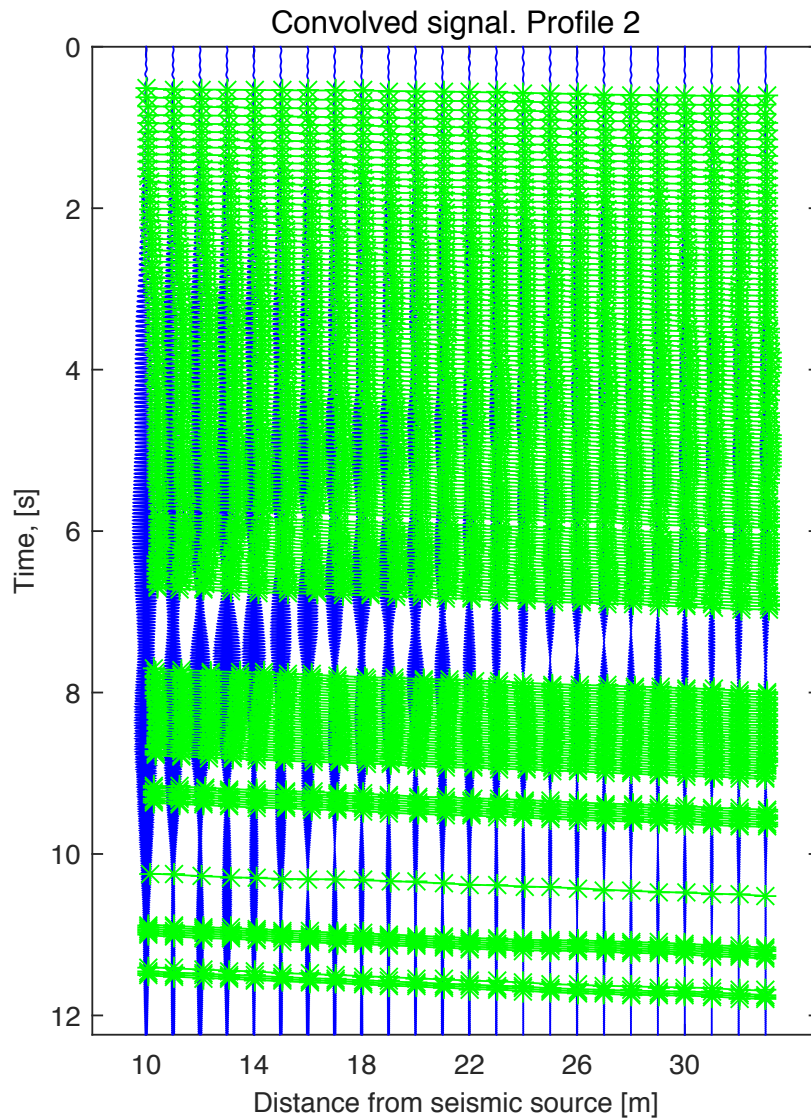
Figure A.11: A 24-channel swept-frequency record with linearly changing frequency from $f_1 = 5$ Hz to $f_2 = 50$ Hz obtained from the impulsive record in Figure A.5 by convolution. Profile 2.

By using the stretch function to linearly separate the frequencies contained in each impulsive record, the phase velocity corresponding to each frequency component can by computed using the previously described methods (see Section 6.1.1). In Figures A.10 and A.11, linear events corresponding to separate frequency components of each record are shown. The resulting dispersion curves, determined based on the linear slopes of each frequency component (line) in Figures A.10 and A.11 are shown in Figures A.12 and A.13.
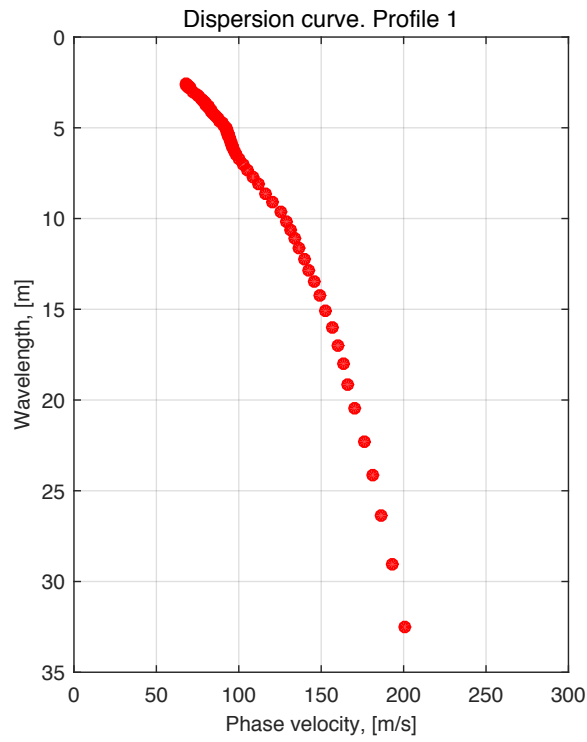
Figure A.12: Fundamental mode dispersion curve obtained from the swept-frequency record in Figure A.10 by using the swept-frequency approach. Profile 1.
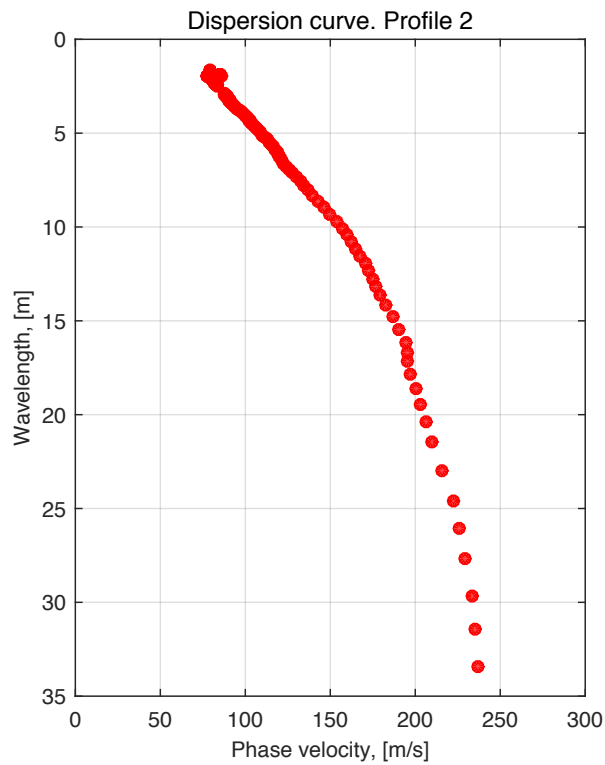

Figure A.13: Fundamental mode dispersion curve obtained from the swept-frequency record in Figure A.11 by using the swept-frequency approach. Profile 2.

A.2.3 Comparison

Figures A.14 and A.15 show comparison of dispersion curves obtained by the swept-frequency approach and the phase-shift method. As indicated by Figures A.14 and A.15, the dispersion curves obtained by the two methods are strictly comparable.
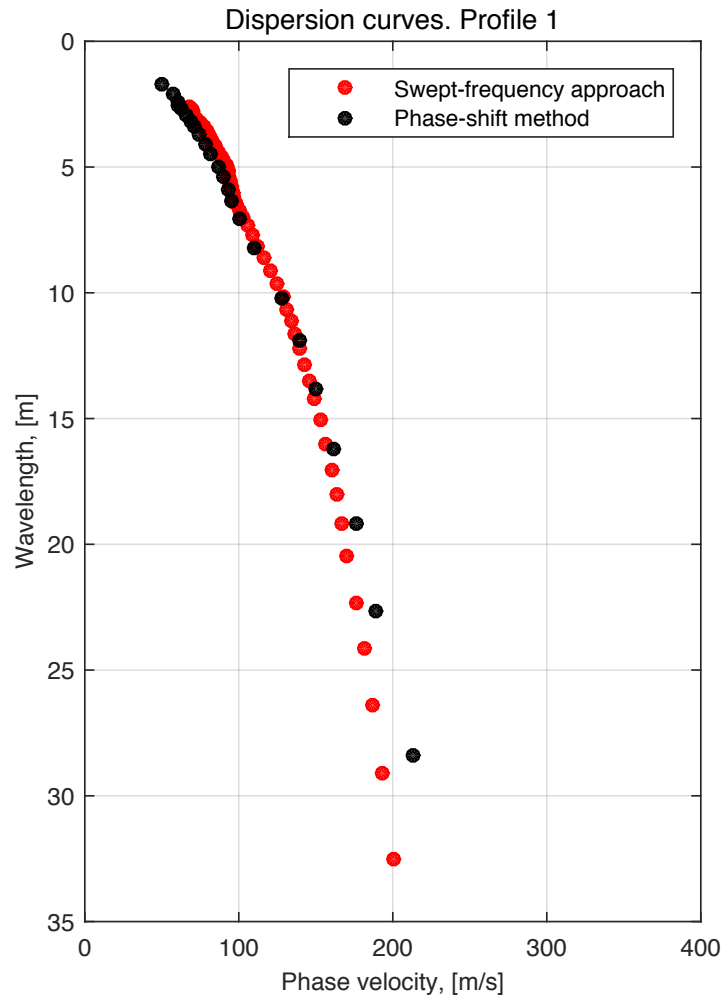

Figure A.14: Comparison of dispersion curves obtained by the phase-shift method and the swept-frequency approach. Profile 1.
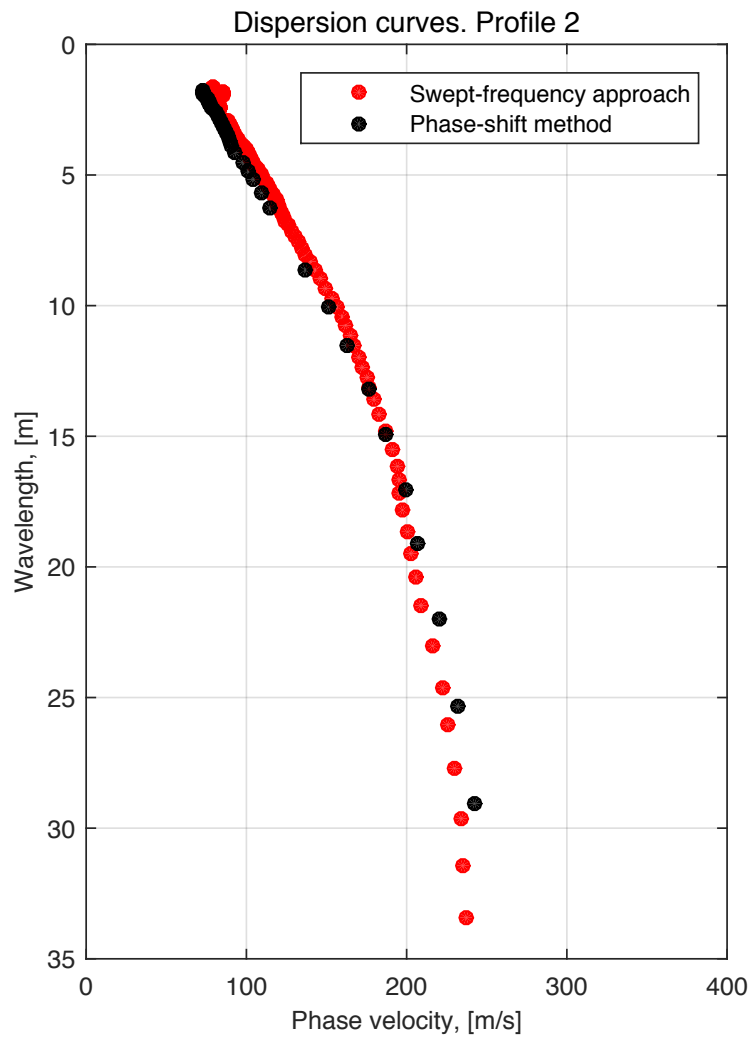
Figure A.15: Comparison of dispersion curves obtained by the phase-shift method and the swept-frequency approach. Profile 2.